rat genes (NetAffx[5]). Upon assignment of orthologs, rat probes sets without human ortholog information were excluded. Because for the redundant probe sets for human samples, a single probe set was selected based on the reliability and dose-dependency of the expression profile. Finally, the probe sets, which were designated as absent by Affymetrix detection, call in seven or more out of eight samples (two each for control and high dose treated in rat and human) were excluded from further analysis.

To facilitate analysis in the large-scale microarray database, we developed two types of one-dimensional score, TGP1 and TGP2, which express the trends in changes in expression of biomarker genes as a whole. The former is based on the signal log ratio[6] and is convenient for comparing the responsiveness of several drugs to a marker gene list. The disadvantages of this scoring system are that it overestimates responsiveness when the list contains a gene for which induction is extreme (such as CYP1A1) and it underestimates responsiveness when genes in the list are mobilized in either direction. To overcome these disadvantages, we used another score, TGP2, which is based on the size of the effects $g = l\mu_2 - \mu_1 l/\sigma_{pooled}$, where

$$\sigma_{pooled} = \sqrt{\frac{(N_1-1)\sigma_1 + (N_2-1)\sigma_2{}^2}{(N_1+N_2-2)}}$$

To obtain an unbiased estimate of the effect size d = c × d, where c is bias correction[7]

$$c = 1 - \frac{3}{4(N_1+N_2-2)-1}$$

The corrected effect size was calculated for each probe set in the marker gene list, summed, and divided by the number of probe sets in the list, and finally multiplied by 100 to obtain the TGP2 score used in the present study.

Results

Changes in rat livers in response to treatment with coumarin

We noted several pathological changes in rat livers after administration of coumarin (Table 1). Twenty-four hour after a single dose of coumarin, no abnormal morphological changes were observed by light microcopy (Figure 1a,b). However, histopathological changes became apparent with repeated administration of coumarin for 1 week or later in the highest dose group, and degenerative lesions, such as vacuolar degeneration and intracytoplasmic inclusion bodies, were evident at day 29 post-initiation of treatment (Figure 1c,d). From day 4 to day 29, single cell necrosis of hepatocytes was occasionally observed.

We next used electron microscopy to look for subtle changes that may be apparent 24 h after a single dose of coumarin. The analysis showed dilation of the rough endoplasmic reticulum of hepatocytes in

Table 1 Histopathological findings in rat livers treated with coumarin

Histopathological findings	*Time Point (days)*	*2*			*4*			*8*			*15*			*29*		
	Dose (mg/kg)	*15*	*50*	*150*	*15*	*50*	*150*	*15*	*50*	*150*	*15*	*50*	*150*	*15*	*50*	*150*
	Number of animals examined	*5*	*5*	*5*	*5*	*5*	*5*	*5*	*5*	*5*	*5*	*5*	*5*	*5*	*5*	*5*
Hepatocyte / Single cell necrosis		0	0	0	0	0	1	0	0	1	0	0	1	0	0	2
very slight							1			1			1			2
Hepatocyte / Inclusion body, intracytoplasmic		0	0	0	0	0	0	0	0	5	0	0	5	0	0	5
very slight										5			2			
slight													3			2
moderate																3
Hepatocyte, centrilobular / Hypertrophy		0	0	0	0	0	0	0	0	3	0	0	5	0	0	5
very slight										3			2			1
slight													3			4
Hepatocyte, centrilobular / Degeneration, vacuolar		0	0	0	0	0	0	0	0	0	0	0	3	0	0	5
very slight													2			
slight													1			5

Vehicle alone or coumarin 15, 50, or 150 mg/kg was administered orally to rats once daily for 1, 3, 7, 14, and 28 days, and the animals were euthanized 24 h after the last dosing, namely, on 2, 4, 8, 15, and 29 days ($n = 5$). The pathological change in the liver was graded into four categories: very slight, slight, moderate, and severe. The number of animals having the morphology at each grade is shown.

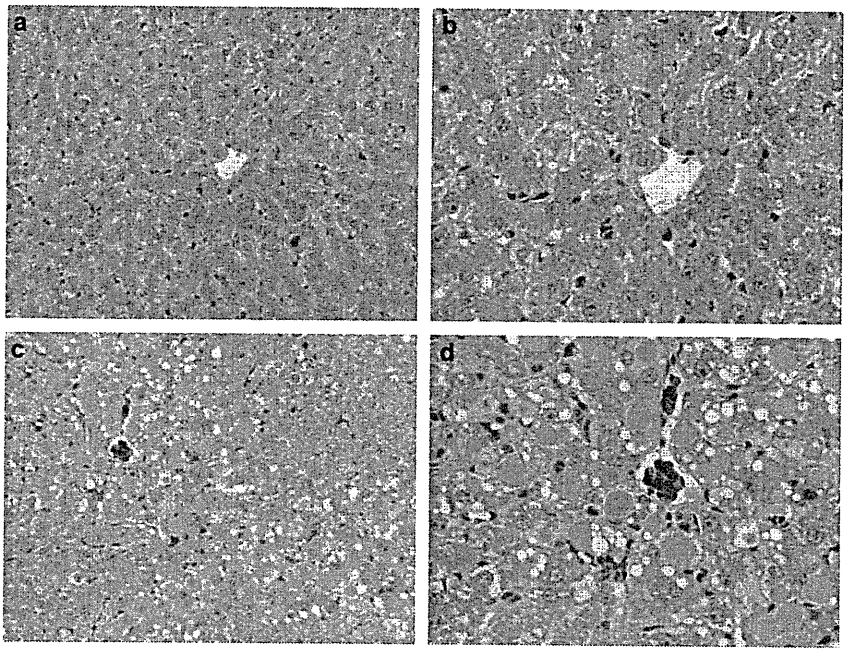

Figure 1 Histopathological changes in the rat liver treated with 150 mg/kg coumarin. (a) Low (×100) and (b) high (×200) magnification micrographs of a liver treated once with 150 mg/kg coumarin (24 h after a single dose). No abnormal morphological changes were detected in the control liver. (c) Low (×100) and (d) high (×200) magnification images of a liver treated with 150 mg/kg coumarin once a day for 28 days. Degenerative changes, such as vacuolation of hepatocytes, are evident after repeated administration of coumarin.

the centrilobular region of the liver in the highest dose group (Figure 2). This early slight ultrastructural change was considered to be consistent with hepatic injury we observed after repeated exposure to the drug. Thus, the 24-h post-treatment time point seemed appropriate for microarray analysis, as at the cellular level, coumarin had already begun exerting an effect at 24-h post-single treatment.

As described in the Methods section, statistically significant up- (136 probe sets) and down-regulated genes (79 probe sets) were extracted and these are listed in Tables 2 and 3. In livers treated with coumarin, the following genes were remarkably mobilized, that is, genes involved in glutathione metabolism and oxidative stress: "glutathione reductase", "glutathione-S-transferase, pi 1/2", "glutathione S-transferase Yc2 subunit", "microsomal glutathione S-transferase 2", "glutamate-cysteine ligase, catalytic subunit", "glutamate-cysteine ligase, modifier subunit", "aldo-keto reductase family 7, member A3

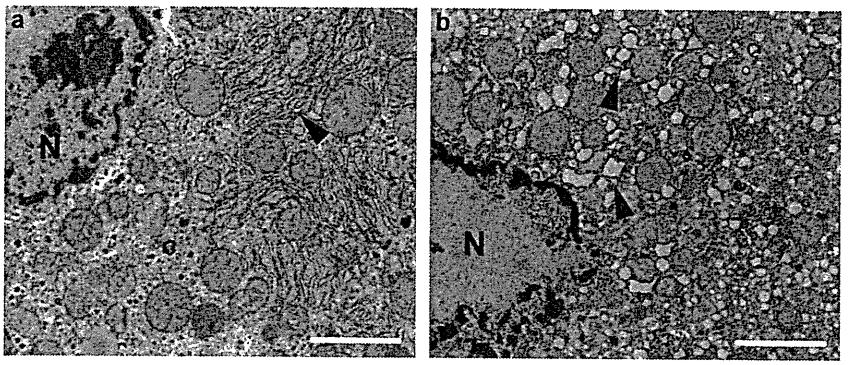

Figure 2 Early detection of coumarin-induced changes by electron microscopy. (a) Control hepatocyte, (b) coumarin-treated hepatocyte (150 mg/kg; 24 h after a single dose). Expansion of the rough endoplasmic reticulum (rER) in the coumarin-treated hepatocyte as compared with a control is evident. N, nucleus; Arrowhead, rER; Bar = 2 μm.

Table 2 Genes up-regulated in the rat liver 24 h after administration of coumarin

Affymetrix probe set ID	*Gene symbol*	*Gene description*	*Fold change*		
			Dose (mg/kg)		
			15	*50*	*150*
1371817_at	LOC290651	Similar to myo-inositol 1-phosphate synthase A1	9.52		26.50
1388122_at	Gstp1/Gstp2	Glutathione-S-transferase, pi 1/pi 2	2.84	1.57	13.00
1369698_at	Abcc3	ATP-binding cassette, sub-family C (CFTR/MRP), member 3	4.41	2.59	11.58
1370342_at	Kcnk2	Potassium channel, subfamily K, member 2	2.45	3.22	10.87
1368013_at	Ddit4l	DNA-damage-inducible transcript 4-like	1.71	1.41	9.07
1388271_at	LOC682651/LOC689415	Similar to Metallothionein-2 (MT-2) (Metallothionein-II) (MT-II)	1.39	1.40	8.81
1375213_at	Pck2_predicted	Phosphoenolpyruvate carboxykinase 2 (mitochondrial) (predicted)	3.07	1.97	6.09
1371237_a_at	Mt1a	Metallothionein 1a	1.52	1.70	5.92
1368121_at	Akr7a3	Aldo-keto reductase family 7, member A3 (aflatoxin aldehyde reductase)	3.43	2.00	5.78
1387599_a_at	Nqo1	NAD(P)H dehydrogenase, quinone 1	2.68	2.33	5.77
1371970_at	RGD1560913_predicted	Similar to expressed sequence AW413625 (predicted)	2.92	1.19	5.67
1371089_at	—	Transcribed locus	2.25	1.38	5.29
1379740_at	LOC361346	Similar to chromosome 18 open reading frame 54	2.29	2.32	4.96
1387693_a_at	Slc6a9	Solute carrier family 6 (neurotransmitter transporter, glycine), member 9	1.66	0.97	4.94
1372510_at	Srxn1	Sulfiredoxin 1 homolog	1.19	0.95	4.91
1370902_at	Akr1b8	Aldo-keto reductase family 1, member B8	2.20	1.96	4.69
1369772_at	Slc6a9	Solute carrier family 6 (neurotransmitter transporter, glycine), member 9	1.45	0.92	4.42
1368247_at	Hspa1a /Hspa1b	Heat shock 70kD protein 1A/1B (mapped)	2.18	1.94	4.22
1387925_at	Asns	Asparagine synthetase	1.40	1.35	4.06
1376051_at	Cryl1	Crystallin, lamda 1	1.25	1.24	3.94
1367847_at	Nupr1	Nuclear protein 1	1.24	1.46	3.86
1368143_at	Anxa7	Annexin A7	1.68	1.38	3.77
1377016_at	Creld2	Cysteine-rich with EGF-like domains 2	0.88	0.94	3.75
1373043_at	LOC680945/LOC683036	Similar to stromal cell–derived factor 2-like 1	1.86	1.99	3.71
1388102_at	Ltb4dh	Leukotriene B4 12-hydroxydehydrogenase	1.44	1.05	3.59
1372653_at	Fkbp11	FK506 binding protein 11	1.64	1.42	3.54
1373810_at	Pla2g12a_predicted	Phospholipase A2, group XIIA (predicted)	1.42	1.96	3.53
1376247_at	—	Transcribed locus	1.97	1.39	3.52
1371442_at	Hyou1	Hypoxia up-regulated 1	1.26	0.88	3.50
1372985_at	Zfp444_predicted	Zinc finger protein 444 (predicted)	2.10	1.28	3.47
1373787_at	Slc6a9	Solute carrier family 6 (neurotransmitter transporter, glycine), member 9	1.35	1.02	3.30
1394080_at	—	Transcribed locus	2.66	2.54	3.17
1373850_at	Smpdl3b	Sphingomyelin phosphodiesterase, acid-like 3B	1.46	1.23	3.07
1370073_at	Dnajc3	Protein kinase inhibitor p58	1.53	1.31	3.06
1374036_at	Mcm2_predicted	Minichromosome maintenance deficient 2 mitotin (predicted)	1.55	0.85	3.06
1370912_at	Hspa1b	Heat shock 70kD protein 1B (mapped)	1.64	1.46	3.01
1377145_at	LOC362068	Similar to monogenic, audiogenic seizure susceptibility 1	1.56	1.63	2.99
1392920_at	Ell3	Elongation factor RNA polymerase II-like 3	1.62	1.41	2.96
1376668_at	RGD1311126_predicted	Similar to RIKEN cDNA 4922503N01 (predicted)	0.92	0.79	2.94
1389308_at	Dnajb11	DnaJ (Hsp40) homolog, subfamily B, member 11	1.42	1.14	2.91
1376055_at	Mcm5_predicted	Minichromosome maintenance deficient 5, cell division cycle 46 (predicted)	1.81	1.07	2.90
1375852_at	Hmgcr	3-hydroxy-3-methylglutaryl-Coenzyme A reductase	1.28	0.91	2.90
1386958_at	Txnrd1	Thioredoxin reductase 1	1.07	0.81	2.89
1371210_s_at	RT1-Aw2	RT1 class Ib, locus Aw2	1.50	1.72	2.88
1372390_at	—	Transcribed locus	1.25	0.81	2.86
1374359_at	Ccne2_predicted	Cyclin E2 (predicted)	1.24	0.91	2.85
1370665_at	Hyou1	Hypoxia up-regulated 1	1.03	0.87	2.84
1387212_at	Bhlhb8	Basic helix-loop-helix domain containing, class B, 8	1.51	2.29	2.81
1374805_at	RGD1561749_predicted	Similar to hypothetical protein MGC5528 (predicted)	2.25	1.13	2.81
1389578_at	Isrip	Ischemia/reperfusion inducible protein	1.23	1.25	2.73
1370429_at	RT1-Aw2	RT1 class Ib, locus Aw2	1.89	1.29	2.70
1370803_at	Zwint	ZW10 interactor	1.58	1.23	2.68
1370688_at	Gclc	Glutamate-cysteine ligase, catalytic subunit	1.06	0.64	2.67
1377037_at	LOC679253/LOC681337	Similar to Acyl-coA thioesterase 4	1.32	0.96	2.65
1375428_at	Creg_predicted	Cellular repressor of E1A-stimulated genes (predicted)	1.24	1.17	2.65
1374048_at	Nrtn	Neurturin	1.61	1.63	2.64
1377334_at	RT1-Ba	RT1 class II, locus Ba	1.86	1.85	2.63

(continued)

Table 2 *(continued)*

Affymetrix probe set ID	*Gene symbol*	*Gene description*	*Fold change*		
			Dose (mg/kg)		
			15	*50*	*150*
1388628_at	Tmed3	Transmembrane emp24 domain containing 3	1.40	1.17	2.59
1367733_at	Ca2	Carbonic anhydrase 2	1.11	0.86	2.59
1373557_at	Mcm4	Minichromosome maintenance deficient 4 homolog	1.51	0.90	2.57
1368544_a_at	Nol3	Nucleolar protein 3	1.30	1.67	2.57
1372954_at	—	Sprague-Dawley UV73 mRNA, partial sequence	1.37	1.80	2.54
1369061_at	Gsr	Glutathione reductase	1.27	1.09	2.53
1370007_at	Pdia4	Protein disulfide isomerase associated 4	1.10	0.98	2.53
1389391_at	RGD1564876_predicted	Similar to solute carrier family 35, member E3 (predicted)	1.26	0.98	2.50
1372523_at	Gclc	Glutamate-cysteine ligase, catalytic subunit	1.17	0.79	2.50
1390591_at	Slc17a3	Na/Pi cotransporter 4	1.67	1.07	2.49
1368376_at	Nr0b2	Nuclear receptor subfamily 0, group B, member 2	1.74	1.69	2.49
1398791_at	Txnrd1	Thioredoxin reductase 1	1.10	0.89	2.48
1367938_at	Ugdh	UDP-glucose dehydrogenase	1.28	0.96	2.46
1387022_at	Aldh1a1	Aldehyde dehydrogenase family 1, member A1	2.15	1.21	2.44
1373613_at	LOC300191	Similar to RIKEN cDNA 4930570C03	1.09	0.96	2.44
1372406_at	Mcm3_predicted	Minichromosome maintenance deficient 3 (predicted)	1.65	0.81	2.43
1374121_at	—	Transcribed locus	2.32	1.82	2.41
1372261_at	—	Transcribed locus	1.23	1.13	2.41
1384130_at	RGD1560171_predicted	Similar to PRO0149 protein (predicted)	1.63	2.13	2.39
1380030_at	Znf593_predicted	Zinc finger protein 593 (predicted)	1.09	0.88	2.38
1389671_at	Trpc2	Transient receptor potential cation channel, subfamily C, member 2	1.21	1.29	2.36
1373445_at	Nol8_predicted	Nucleolar protein 8 (predicted)	1.24	0.85	2.36
1387083_at	Ctf1	Cardiotrophin 1	1.18	0.96	2.35
1377135_at	Alox5	Arachidonate 5-lipoxygenase	1.00	1.25	2.34
1375088_at	—	Transcribed locus	0.98	1.14	2.31
1369588_a_at	Atpif1	ATPase inhibitory factor 1	1.27	1.13	2.30
1398341_at	RGD1559720_predicted	RGD1559720 (predicted)	1.03	1.09	2.29
1389767_at	RGD1304924_predicted	Similar to hypothetical protein FLJ31364 (predicted)	1.13	1.18	2.29
1374249_at	RGD1304580	Similar to Hypothetical protein MGC38513	0.93	1.10	2.28
1373530_at	Ccne1	cyclin E	1.06	0.52	2.28
1371113_a_at	Tfrc	Transferrin receptor	1.28	0.76	2.28
1370127_at	Pold1	Polymerase (DNA directed), delta 1, catalytic subunit	1.42	1.37	2.28
1376073_at	Sel1h	Sel1 (suppressor of lin-12) 1 homolog	1.40	1.06	2.26
1392841_at	—	Transcribed locus	1.39	2.02	2.23
1398879_at	Tmem66	Transmembrane protein 66	1.25	1.07	2.22
1388622_at	Nol5a	Nucleolar protein 5A	1.46	1.19	2.22
1371583_at	Rbm3	RNA binding motif protein 3	1.19	1.16	2.21
1387188_at	Slc17a1	Solute carrier family 17, member 1	1.37	1.33	2.20
1368037_at	Cbr1	Carbonyl reductase 1	0.96	1.01	2.20
1390430_at	Nr1d2	Nuclear receptor subfamily 1, group D, member 2	0.97	1.05	2.19
1398788_at	Pdia3	Protein disulfide isomerase associated 3	1.43	1.24	2.19
1386922_at	Ca2	Carbonic anhydrase 2	1.07	0.83	2.19
1367983_at	Fen1	Flap structure–specific endonuclease 1	1.59	1.12	2.16
1373999_at	—	Transcribed locus	1.27	0.83	2.16
1376781_at	Glb1_mapped	Galactosidase, beta 1 (mapped)	1.20	1.03	2.14
1381968_at	Sema6d_predicted	Sema domain, transmembrane domain (TM), and cytoplasmic domain, (semaphorin) 6D (predicted)	1.18	1.20	2.13
1372774_at	Coq6	Coenzyme Q6 homolog	1.30	0.90	2.13
1376098_a_at	Lad1_predicted	Ladinin (predicted)	1.02	1.03	2.12
1370904_at	Hla-dma	Major histocompatibility complex, class II, DM alpha	1.32	1.11	2.12
1389805_at	—	—	1.27	1.29	2.11
1388331_at	Tra1_predicted	Tumor rejection antigen gp96 (predicted)	1.08	0.93	2.11
1386466_at	—	Transcribed locus	1.08	1.24	2.11
1372599_at	Mgst2_predicted	Microsomal glutathione S-transferase 2 (predicted)	1.34	1.34	2.11
1372471_at	—	Transcribed locus	1.66	1.03	2.10
1372247_at	Ddost_predicted	Dolichyl-di-phosphooligosaccharide-protein glycotransferase (predicted)	1.26	1.15	2.10
1370055_at	Rab3d	RAB3D, member RAS oncogene family	0.72	0.77	2.10
1398596_at	—	Transcribed locus	2.07	1.65	2.09
1387783_a_at	Acaa1	Acetyl-coenzyme A acyltransferase 1	1.49	1.20	2.09
1373908_at	—	—	1.71	1.40	2.09
1398383_at	Cyb561_predicted	Cytochrome b-561 (predicted)	1.40	1.15	2.07
1377350_at	—	Transcribed locus	1.74	1.26	2.07
1370428_x_at	RT1-Aw2	RT1 class Ib, locus Aw2	1.66	1.50	2.07

(continued)

Table 2 *(continued)*

Affymetrix probe set ID	*Gene symbol*	*Gene description*	*Fold change*		
			Dose (mg/kg)		
			15	*50*	*150*
1369693_a_at	Slc1a2	Solute carrier family 1, member 2	1.81	1.96	2.07
1370541_at	Nr1d2	Nuclear receptor subfamily 1, group D, member 2	0.91	1.01	2.06
1389004_at	Josd2_predicted	Josephin domain containing 2 (predicted)	1.12	0.95	2.06
1370030_at	Gclm	Glutamate cysteine ligase, modifier subunit	1.06	0.81	2.06
1370000_at	Thra	Thyroid hormone receptor alpha	1.79	1.66	2.06
1370663_at	Wee1	Wee 1 homolog	1.92	1.00	2.05
1390321_at	RGD1304693_predicted	Similar to CG14803-PA (predicted)	1.68	1.15	2.03
1389209_at	RGD1306274	Similar to hypothetical protein BC002942	1.82	1.17	2.03
1388750_at	Tfrc	Transferrin receptor	1.32	0.87	2.03
1373935_at	Pold2	Polymerase (DNA directed), delta 2, regulatory subunit	1.35	1.18	2.03
1390579_at	RGD1305222_predicted	Similar to RIKEN cDNA 1810029B16 (predicted)	0.84	0.70	2.02
1389889_at	RGD1306404_predicted	Similar to mKIAA1402 protein (predicted)	1.21	1.03	2.02
1373499_at	Gas5	Growth arrest specific 5	1.15	1.03	2.02
1373386_at	Gjb2	Gap junction membrane channel protein beta 2	0.81	1.08	2.02
1376001_at	Praf1_predicted	Polymerase (RNA) I associated factor 1 (predicted)	1.17	0.98	2.01
1373200_at	Eef1e1_predicted	Eukaryotic translation elongation factor 1 epsilon 1 (predicted)	1.19	1.25	2.01
1380854_at	R3hdm1	R3H domain containing 1	1.20	1.28	2.00

Probe sets are sorted by fold change. Shaded probe sets, those selected as in-vivo–in-vitro bridging probes (see Figure 3).

(aflatoxin aldehyde reductase)", "NAD(P)H dehydrogenase, quinone 1", "thioredoxin reductase 1", and "metallothionein"; genes related to the heat shock response: "crystallin, lamda 1", "DnaJ (Hsp40) homolog, subfamily B, member 11", "heat shock 70kD protein 1A/1B", and "protein kinase inhibitor p58"; genes responsive to hypoxia: "hypoxia up-regulated 1" and "ischemia/reperfusion inducible protein"; and genes related to DNA repair and the cell cycle: "DNA-damage-inducible transcript 4-like", "cyclin E", "growth arrest specific 5", and "wee 1 homolog". Changes in expression of these genes in hepatocytes can be interpreted as a reflection of the adaptive response to oxidative stress and cellular damage. Among the extracted genes, the following genes appeared to be the most sensitive to coumarin, "aldo-keto reductase family 7, member A3", "NAD(P)H dehydrogenase, quinone 1", "glutathione reductase", "glutathione-S-transferase, pi 1/2", and "glutathione S-transferase Yc2 subunit", as they were remarkably mobilized at the lowest dose of coumarin-treatment (15 mg/kg).

Comparison between in-vivo and in-vitro rat hepatocyte responses

Primary cultured rat hepatocytes were exposed to 12, 60, and 300 μM coumarin for 24 h. No obvious cytotoxicity was detected by LDH release (100.5, 97.7, and 95.1% of control, respectively). In case of the in-vitro system, statistical filtering was not appropriate because the data were the duplicate measurements from a single rat. We then extracted the significant genes according to the gene list obtained from in-vivo study, that is, the genes showing significant up- (136 probe sets) or down-regulation (79 probe sets) in livers treated with 150 mg/kg coumarin. As shown in Figure 3a, a similar trend was observed between in-vivo and in-vitro cell responses, although the extent of the response (i.e., fold change) was generally smaller, and fewer genes showed a measurable change in the in-vitro cell assay. Probe sets showing changes of 1.5-fold or more and 0.6-fold or less than that of control at the highest concentration (300 μM) in rat hepatocytes were selected as those reflecting the toxicological mechanism of coumarin *in vivo*, namely, "in-vivo–in-vitro bridging probes". For the selected genes (37 up-regulated and 29 down-regulated; see shading in Tables 2 and 3), clear dose-dependent changes in expression were observed (Figure 3b), and the observation enabled us to assess hepatotoxicity of coumarin using the in-vitro data.

Comparison between rat and human hepatocytes

Cultured human hepatocytes were also exposed to 12, 60, and 300 μM coumarin for 24 h. No obvious cytotoxicity was detected by LDH release (100.6, 100.9, and 102.0% of control, respectively). The in-vivo–in-vitro bridging probes were assigned to their human ortholog genes to form a set of "rat–human bridging probes" and changes in their expression were compared in rat versus human hepatocytes. In total, 14 up-regulated and 11 down-regulated probe sets were identified and their relative expression levels are shown as a heatmap in Figure 4. It appears that the pattern of changes in gene expres-

Table 3 Genes down-regulated in the rat liver 24 h after administration of coumarin

Affymetrix probe set ID	*Gene symbol*	*Gene description*	*Fold change*		
			Dose (mg/kg)		
			15	*50*	*150*
1386977_at	Ca3	Carbonic anhydrase 3	0.64	1.01	0.13
1370778_at	LOC259245	Alpha-2u globulin	0.87	0.84	0.16
1386474_at	—	Transcribed locus	1.53	0.59	0.19
1393902_at	Akr1c6	Aldo-keto reductase family 1, member C6	0.42	0.53	0.20
1375900_at	LOC500590	Similar to T-cell antigen 4-1BB precursor – mouse	0.56	0.52	0.21
1371412_a_at	Nrep	Neuronal regeneration related protein	0.86	0.88	0.25
1387491_at	Gyk	Glycerol kinase	0.76	0.72	0.28
1376637_at	—	Transcribed locus	0.62	1.03	0.29
1373722_at	Kif20a_predicted	Kinesin family member 20A (predicted)	1.12	0.91	0.29
1367896_at	Ca3	Carbonic anhydrase 3	0.80	0.98	0.29
1385247_at	Ugt2b	UDP glycosyltransferase 2 family, polypeptide B	0.68	0.04	0.31
1387852_at	Thrsp	Thyroid hormone–responsive protein	1.06	0.87	0.32
1393221_at	RGD1564865_predicted	Similar to 20-alpha-hydroxysteroid dehydrogenase (predicted)	0.67	0.97	0.32
1387665_at	Bhmt	Betaine-homocysteine methyltransferase	0.81	1.18	0.33
1387185_at	Apbb3	Amyloid beta (A4) precursor protein-binding, family B, member 3	0.84	0.84	0.33
1387053_at	Fmo1	Flavin containing monooxygenase 1	0.62	0.79	0.34
1398286_at	Csad	Cysteine sulfinic acid decarboxylase	1.07	0.92	0.34
1387655_at	Cxcl12	Chemokine (C-X-C motif) ligand 12	0.67	0.45	0.34
1368458_at	Cyp7a1	Cytochrome P450, family 7, subfamily a, polypeptide 1	0.78	0.69	0.36
1388583_at	Cxcl12	Chemokine (C-X-C motif) ligand 12	0.77	0.67	0.37
1387243_at	Cyp1a2	Cytochrome P450, family 1, subfamily a, polypeptide 2	0.78	0.90	0.37
1387139_at	Hao2	Hydroxyacid oxidase 2 (long chain)	0.79	1.15	0.37
1373006_at	Prp2	Proline-rich protein PRP2	0.70	0.79	0.37
1370026_at	Cryab	Crystallin, alpha B	1.01	0.71	0.37
1390443_at	—	Transcribed locus	0.88	0.75	0.38
1375144_at	—	Transcribed locus	1.02	0.52	0.39
1369044_a_at	Pde4b	Phosphodiesterase 4B	0.59	0.64	0.39
1370057_at	Csrp1	Cysteine and glycine-rich protein 1	0.93	0.90	0.39
1369450_at	Ust5r	Integral membrane transport protein UST5r	0.74	0.94	0.39
1367729_at	Oat	Ornithine aminotransferase	0.63	1.00	0.39
1374677_at	LOC684425	Similar to adenylosuccinate synthetase isozyme 1	0.80	1.00	0.40
1388038_at	Atrn	Attractin	0.88	0.88	0.40
1388031_x_at	LOC259245/Mup5	Alpha-2u globulin	0.70	0.95	0.40
1370150_a_at	Thrsp	Thyroid hormone–responsive protein	1.03	0.97	0.41
1390450_a_at	Ogn_predicted	Osteoglycin (predicted)	0.63	0.53	0.41
1369664_at	Avpr1a	Arginine vasopressin receptor 1A	0.88	0.87	0.41
1388433_at	Krt1-19	Keratin complex 1, acidic, gene 19	1.09	0.71	0.42
1371400_at	Thrsp	Thyroid hormone–responsive protein	1.04	0.98	0.42
1369296_at	Sult1c1	Sulfotransferase family, cytosolic, 1C, member 1	0.86	1.13	0.42
1389728_at	—	—	0.77	0.56	0.42
1389188_at	Gpr108	G protein-coupled receptor 108	0.69	0.53	0.42
1380546_at	LOC298250	Similar to hypothetical protein FLJ10986	0.87	0.89	0.42
1376427_a_at	Gldc_predicted	Glycine decarboxylase (predicted)	0.85	0.88	0.42
1372685_at	Cdkn3_predicted	Cyclin-dependent kinase inhibitor 3 (predicted)	1.03	1.14	0.42
1369546_at	Bbox1	Butyrobetaine (gamma), 2-oxoglutarate dioxygenase 1	0.90	0.82	0.42
1389566_at	Ccnb2	Cyclin B2	1.13	1.11	0.43
1374157_at	Rgs8	Regulator of G-protein signaling 8	0.76	0.61	0.43
1398282_at	Kynu	Kynureninase (L-kynurenine hydrolase)	0.73	0.96	0.44
1387816_at	Igfals	Insulin-like growth factor binding protein, acid labile subunit	1.09	0.77	0.45
1387528_at	Mbl2	Mannose binding lectin 2, protein C	0.77	0.86	0.45
1387372_at	Slc6a13	Solute carrier family 6, member 13	0.89	0.75	0.45
1376311_at	RGD1563465_predicted	Similar to netrin G1 (predicted)	0.79	0.29	0.45
1374072_at	LOC689898	Hypothetical protein LOC689898	0.97	0.62	0.45
1370355_at	Scd1	Stearoyl-coenzyme A desaturase 1	1.56	1.13	0.45
1368627_at	Rgn	Regucalcin	0.85	0.91	0.45
1387203_at	Gckr	Glucokinase regulatory protein	0.79	1.01	0.46
1388425_at	RGD1305890	Similar to RIKEN cDNA D130038B21	0.83	0.78	0.46
1377412_at	—	Transcribed locus	0.91	0.67	0.46
1377375_at	Aass_predicted	Aminoadipate-semialdehyde synthase (predicted)	0.98	0.80	0.46
1374760_at	—	Transcribed locus	0.76	1.07	0.46
1373967_at	—	Transcribed locus	0.87	0.77	0.46
1367979_s_at	Cyp51	Cytochrome P450, subfamily 51	0.92	0.77	0.46
1367939_at	Rbp1	Retinol binding protein 1, cellular	0.62	0.90	0.46

(continued)

Table 3 *(continued)*

Affymetrix probe set ID	*Gene symbol*	*Gene description*	*Fold change*		
			Dose (mg/kg)		
			15	*50*	*150*
1394068_x_at	Klf2_predicted	Kruppel-like factor 2 (lung) (predicted)	0.74	0.70	0.47
1389681_at	Pvrl2	Poliovirus receptor-related 2	0.88	0.97	0.47
1387307_at	Hal	Histidine ammonia lyase	0.87	0.76	0.47
1373814_at	RGD1310066	Similar to mKIAA1002 protein	0.80	0.84	0.47
1390672_at	Rprm	Candidate mediator of the p53-dependent G2 arrest	0.83	0.79	0.48
1367857_at	Fads1	Fatty acid desaturase 1	1.06	0.93	0.48
1387328_at	Cyp2c	Cytochrome P450, subfamily IIC (mephenytoin 4-hydroxylase)	0.80	1.06	0.48
1386975_at	Pdk2	Pyruvate dehydrogenase kinase, isoenzyme 2	0.61	0.65	0.48
1376785_at	Sycp3	Synaptonemal complex protein 3	0.70	0.85	0.48
1367804_at	Apcs	Serum amyloid P-component	0.70	0.78	0.48
1398759_at	Tgfb1i4	Transforming growth factor beta 1 induced transcript 4	0.72	0.83	0.49
1386041_a_at	Klf2_predicted	Kruppel-like factor 2 (lung) (predicted)	0.83	0.63	0.49
1375599_at	Ddx31_predicted	DEAD/H (Asp-Glu-Ala-Asp/His) box polypeptide 31 (predicted)	0.86	0.57	0.49
1388300_at	Mgst3_predicted	Microsomal glutathione S-transferase 3 (predicted)	0.69	1.00	0.50
1368733_at	Ste	Sulfotransferase, estrogen preferring	0.88	0.98	0.50
1368227_at	Slc28a2	Solute carrier family 28, member 2	1.05	0.84	0.50

Probe sets are sorted by fold change. Shaded probe sets are the ones selected as in-vivo–in-vitro bridging probes (see Figure 3).

sion is similar in rat and human cells but that the extent of the changes is more prominent in rat cells than in human cells. Among them, "protein kinase inhibitor p58", "DnaJ (Hsp40) homolog, subfamily B, member 11", "crystallin, lamda 1", "hypoxia up-regulated 1", and "aldo-keto reductase family 7, member A3 (aflatoxin aldehyde reductase)", which showed remarkable expression changes both in rat *in vivo* and *in vitro*, did not show any significant changes in human hepatocytes. As for the genes such as "ischemia/reperfusion inducible protein", "glutathione reductase", "glutamate-cysteine ligase, catalytic subunit", "NAD(P)H dehydrogenase, quinone 1", and "DNA-damage-inducible transcript 4-like", these were up-regulated in both species, but the extent of up-regulation was much less in human cells than in the rat.

In the next step, changes in expression of these were examined in cells treated with another hepatotoxicant, DFNa, which is known to elicit a similar response as does coumarin, that is, oxidative stress and glutathione depletion.[8,9] Although not all the genes showed changes in common with those observed after coumarin treatment, the trend appeared similar, suggesting that both compounds share the same toxicological pathway(s).

To make a quantitative comparison of responsiveness of the marker genes between species, the mean value of the effect size of the probe sets (TGP2 score) was calculated (Figure 5). It is obvious from the results presented in Figure 5a that the score shows a good dose-dependency, suggesting that the score successfully expresses the responsiveness of cells to the toxicant. Moreover, in the case of coumarin, the score of human hepatocytes to the marker genes is a much lower value than the score observed for rat cells, supporting the known species-specific difference. However, both rat and human cells responded to the markers to the same extent at the same concentration of DFNa. For genes such as "ischemia/reperfusion inducible protein" and "hypoxia up-regulated 1", these were up-regulated in both species at a high-dose DFNa exposure (data not shown). This clearly indicates that the marker genes respond similarly in rat and human hepatocytes when a drug with a similar level of toxicity in each species is applied.

Discussion

Coumarin is a toxin found in many plants, including the tonka bean, and it has clinical value as the precursor for several anticoagulants, especially warfarin. Although coumarin has a sweet scent, its use as a food additive is restricted because of its hepatotoxicity. It is well known that coumarin is a non-genotoxic hepatocarcinogen in rats, whereas such a property has not been probed in other species.[10] The mechanism of coumarin toxicity has been extensively studied and elucidated; it produces oxidative stress leading to glutathione depletion.[11–13] The species-specific difference between rat and human responses to coumarin has been explained as a difference in detoxification after metabolic activation.[14,15]

In most species, including humans, coumarin is hydroxylated by CYP2A to 7-hydroxycoumarin

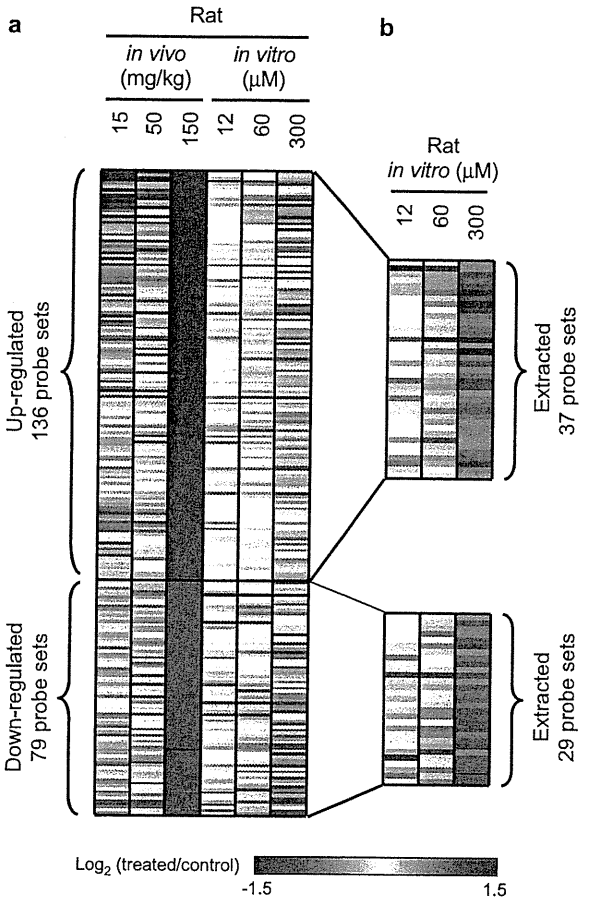

Figure 3 Heatmap of the expression profiles of probe sets in rat liver and rat hepatocytes treated with coumarin. (a) Heatmap of the changes in gene expression induced by coumarin treatment in the in-vivo rat liver (15, 50, 150 mg/kg) and in-vitro hepatocytes (12, 60, and 300 μM). Probes sets were statistically extracted from the data presented in Tables 2 and 3. b: Probe sets with >1.5-fold or <0.6-fold change in rat hepatocytes (the specific sub-set grouped as in-vivo–in-vitro bridging probes are indicated by shading in Tables 2 and 3).

(7-HC), a non-toxic metabolite. In rats, however, CYP2A has a stronger affinity for testosterone than for coumarin, such that 7HC levels are extremely low in this species. Another influencing factor is that in rats, coumarin is converted to coumarin 3,4-epoxide (CE), a reactive intermediate that is detoxified via glutathione conjugation and excreted as a conjugate. When the amount of the active metabolite exceeds the cellular capacity for glutathione conjugation, cell injury may occur. However, there is some evidence to suggest that this pathway is of minor importance to hepatotoxicity, as mouse-liver microsomes show hepatic clearance of coumarin via the epoxide intermediate at levels four times greater than that in rats,[16] but hepatotoxicity is not induced by coumarin treatment in mice. CE is spontaneously converted to another toxic compound, *o*-hydroxyphenylacetaldehyde (*o*-HPA). It has been found that *o*-HPA is rapidly detoxified to *o*-hydroxyphenylacetic acid in mice and humans, whereas this pathway works little in rats.[16,17] Therefore, the difference in *o*-HPA detoxification is currently considered to be the main cause of species-specific differences in sensitivity to coumarin.

The main purpose of the present study was to explore a possible strategy for overcoming the problem of species-specific differences in toxicity that affect testing of potential toxins and therapeutic treatments. Specifically, we were interested to test a toxicogenomics-based approach to address species-specific differences in response to toxins. In the livers of rats treated with coumarin, changes in gene expression were observed in various known genes, possibly reflecting a response to oxidative stress, cell injury, and glutathione depletion, and these coumarin-responsive genes seem likely to be related to the hepatotoxic mechanism of coumarin. Of the coumarin-responsive gene identified in the in-vivo rat liver assay, not all but a considerable numbers of the genes were found to be common to those that were coumarin-responsive in the in-vitro assay, with an observable dose-dependency. The present results suggest that whole-transcriptome analysis of the response can be used to estimate the hepatotoxicity of coumarin using the in-vitro rat hepatocytes. In our experience with other compounds, we found that some chemicals showed a considerably different gene expression profile *in vivo* and *in vitro*,[6] whereas the results with coumarin suggest that it is possible to build a reasonable bridge between rat and human responses using an in-vitro cell assay system.

The responsive genes in common to the in-vivo and in-vitro assay datasets were used to identify human ortholog genes useful for making a comparison between rat and human responses. As it is obvious from the results presented in Figure 4, the trend in changes in expression was similar in both species, but the extent of the changes was generally smaller in human cells than in rat cells in accordance with the known species-specific difference in hepatotoxicity. The observation that induction of stress-related genes and glutathione metabolism–related genes was more robust in rat cells than in human cells could be a direct reflection of the extent of stress and subsequent damage caused by coumarin in each species. The genes "Protein kinase inhibitor p58", "DnaJ (Hsp40) homolog, subfamily B, member 11", "crystallin, lamda 1", "hypoxia up-regulated 1", and "aflatoxin aldehyde reductase" were extensively

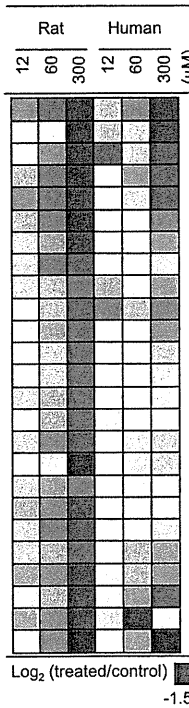

RAE230 2.0	HG-U133 2.0	Gene description (RAE230 2.0)	Gene symbol
1387053_at	205666_at	flavin containing monooxygenase 1	Fmo1
1387243_at	207608_x_at	cytochrome P450, family 1, subfamily A, polypeptide 2	Cyp1a2
1367896_at	204865_at	carbonic anhydrase 3	Ca3
1387139_at	231156_at	hydroxyacid oxidase 2 (long chain)	Hao2
1388583_at	203666_at	chemokine (C-X-C motif) ligand 12	Cxcl12
1387816_at	215712_s_at	insulin-like growth factor binding protein, acid labile subunit	Igfals
1387852_at	229477_at	thyroid hormone responsive protein	Thrsp
1387665_at	206119_at	betaine-homocysteine methyltransferase	Bhmt
1387528_at	207256_at	mannose-binding lectin 2, protein C	Mbl2
1369044_a_at	211302_s_at	phosphodiesterase 4B	Pde4b
1367857_at	208962_s_at	fatty acid desaturase 1	Fads1
1370073_at	208499_s_at	protein kinase inhibitor p58	Dnajc3
1389308_at	223054_at	DnaJ (Hsp40) homolog, subfamily B, member 11	Dnajb11
1390591_at	207298_at	Na/Pi cotransporter 4	Slc17a3
1370665_at	200825_s_at	hypoxia up-regulated 1	Hyou1
1368121_at	206469_x_at	aldo-keto reductase family 7, member A3 (aflatoxin aldehyde reductase)	Akr7a3
1376051_at	220753_s_at	crystallin, lamda 1	Cryl1
1370688_at	202922_at	glutamate-cysteine ligase, catalytic subunit	**Gclc**
1389578_at	218647_s_at	ischemia/reperfusion inducible protein	Yrdc
1369061_at	225609_at	glutathione reductase	Gsr
1373810_at	223373_s_at	phospholipase A2, group XIIA (predicted)	Pla2g12a
1387599_a_at	201468_s_at	NAD(P)H dehydrogenase, quinone 1	Nqo1
1370902_at	206561_s_at	aldo-keto reductase family 1, member B8	Akr1b8
1368013_at	228057_at	DNA-damage-inducible transcript 4-like	**Ddit4l**
1368247_at	200800_s_at	heat shock 70kD protein 1A/1B	**Hspa1a/1b**

Figure 4 Heatmap of the expression profile of probe sets in rat and human hepatocytes treated with coumarin. Among the set of in-vivo–in-vitro bridging probes for rats, 14 up-regulated and 11 down-regulated probe sets were assigned human orthologs (species bridging markers) and their expression is shown as a heatmap that includes the expression profiles in rat and human hepatocytes treated with 12, 60, or 300 μM coumarin. Note that each probe set responded dose-dependently to coumarin in both species, whereas the extent of the changes appears to be more prominent in rat than in human cells.

up-regulated in rats both *in vivo* and *in vitro*, whereas almost no change was observed in these genes in human hepatocytes. It will likely be interesting to determine if the gene sets include genes involved in the cause of the species-specific responses that lead to differences in hepatotoxicity and those genes not involved in the response to coumarin. Clearly, it will be necessary to perform additional experiments to address this question.

We next explored the utility of a score, the TGP2-score that is aimed at quantifying responsiveness of a set of marker genes. The TGP2-score is the average of the effect size on gene expression. When species-specific differences in drug-induced gene expression changes are examined, we often encounter clusters of genes, possibly related to toxicological function, that are affected by the drug in both species tested but in different directions (i.e., up-regulated in one but down-regulated in the other). If responsiveness is quantified by taking account of the direction of changes, we might underestimate the extent to which the set of genes affected are similar. Using the TGP2-score, we estimate responsiveness of a given species when expression of a gene in the analysis set is mobilized in either direction. In the present case, however, the direction of expression change was in common between two species in most or all cases, such that the factor did not contribute much to the scores. The score is also clearly useful to visualize quantitative responsiveness of a set of genes to a toxicant (Figure 5) and a prediction of species-specific difference can also be represented (i.e., the higher toxicity of coumarin in rat than in humans or the lack of a species-specific difference in the case of toxicity of DFNa; Figure 5). It also follows that the genes selected in this study may be useful in-vitro markers of oxidative stress–related hepatocyte injury in both rats and humans and that differential responses in these marker genes are indicative of a species-specific difference.

In conclusion, we successfully used a toxicogenomics approach to reproduce the known species-specific difference in hepatotoxicity of coumarin between rats and humans using an in-vitro hepatocyte culture system and microarray analysis. The application of this approach to other chemicals in our database should reveal other examples that can build bridges between species or suggest other strategies for bridging information among species. The most important mission for a toxicologist interested

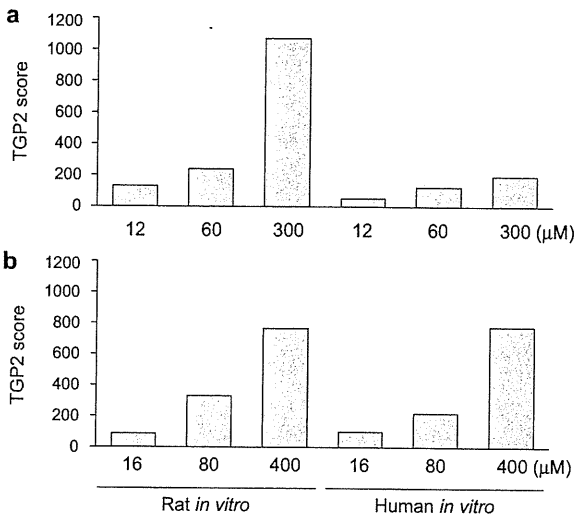

Figure 5 The responsiveness of rat and human hepatocytes expressed as a score based on the effect size (TGP2 score). The expression of each probe set in the set of rat–human bridging probes (Figure 4) was converted to a TGP2 score as described in "Materials and methods" to quantify the responsiveness of each species. (a) Responsiveness to coumarin. Note that the score shows a clear dose-dependency and the expected species-specific difference, that is, rat hepatocytes are more sensitive than human hepatocytes. (b) Responsiveness to diclofenac sodium, a known hepatotoxicant that causes oxidative stress but does not show a species-specific difference in hepatotoxicity. Again, a dose-dependent increase in the score is observed but in this case, as expected, no species-specific difference is observed.

in drug development is to make a precise prediction of the potential clinical toxicity based on animal studies. Toxicogenomics-based approaches are emerging as a promising new avenue of study for making the most of the results of animal studies.

Acknowledgement

This study was supported by a grant from the Ministry of Health, Labour and Welfare of Japan (H14-toxico-001).

References

1 Urushidani, T, Nagao, T. Toxicogenomics: the Japanese initiative. In: Borlak, J, (Ed.), *Handbook of toxicogenomics – strategies and applications. Wiley: VCH*; 2005. p. 623–31.

2 Takashima, K, Mizukawa, Y, Morishita, K, Okuyama, M, Kasahara, T, Toritsuka, N, *et al.* Effect of the difference in vehicles on gene expression in the rat liver-analysis of the control data in the Toxicogenomics Project Database. *Life Sci* 2006; **78**: 2787–2796.

3 Waters, MD, Fostel, JM. Toxicogenomics and systems toxicology: aims and prospects. *Nat Rev Genet* 2004; **5**: 936–948.

4 Mattingly, CJ, Colby, GT, Forrest, JN, Boyer, JL. The Comparative Toxicogenomics Database (CTD). *Environ Health Perspect* 2003; **111**: 793–795.

5 Liu, G, Loraine, AE, Shigeta, R, Cline, M, Cheng, J, Valmeekam, V, *et al.* NetAffx: Affymetrix probesets and annotations. *Nucleic Acids Res* 2003; **31**: 82–86.

6 Kiyosawa, N, Shiwaku, K, Hirode, M, Omura, K, Uehara, T, Shimizu, T, *et al.* Utilization of a one-dimensional score for surveying chemical-induced changes in expression levels of multiple biomarker gene sets using a large-scale toxicogenomics database. *J Toxicol Sci* 2006; **31**: 433–448.

7 Hedges, LV. Distribution theory for Glass's estimator of effect size and related estimators. *J Edu Statis* 1981; **6**: 107–128.

8 Gomez-Lechon, MJ, Ponsoda, X, O'Connor, E, Donato, T, Castell, JV, Jover, R. Diclofenac induces apoptosis in hepatocytes by alteration of mitochondrial function and generation of ROS. *Biochem Pharmacol* 2003; **66**: 2155–2167.

9 Amin, A, Hamza, AA. Oxidative stress mediates drug-induced hepatotoxicity in rats: a possible role of DNA fragmentation. *Toxicology* 2005; **208**: 367–375.

10 National Toxicology Program. NTP toxicology and carcinogenesis studies of coumarin (CAS No. 91-64-5) in F344/N rats and B6C3F1 mice (Gavage Studies). *Natl Toxicol Program Tech Rep Ser* 1993; **422**: 1–340.

11 Lake, BG. Investigations into the mechanism of coumarin-induced hepatotoxicity in the rat. *Arch Toxicol Suppl* 1984; **7**: 16–29.

12 Lake, BG, Gray, TJ, Evans, JG, Lewis, DF, Beamand, JA, Hue, KL. Studies on the mechanism of coumarin-induced toxicity in rat hepatocytes: comparison with dihydrocoumarin and other coumarin metabolites. *Toxicol Appl Pharmacol* 1989; **97**: 311–323.

13 Kiyosawa, N, Uehara, T, Gao, W, Omura, K, Hirode, M, Shimizu, T, *et al.* Identification of glutathione depletion-responsive genes using phorone-treated rat liver. *J Toxicol Sci* 2007; **32**: 469–486.

14 Vassallo, JD, Hicks, SM, Daston, GP, Lehman-McKeeman, LD. Metabolic detoxification determines species differences in coumarin-induced hepatotoxicity. *Toxicol Sci* 2004; **80**: 249–257.

15 Felter, SP, Vassallo, JD, Carlton, BD, Daston, GP. A safety assessment of coumarin taking into account species-specificity of toxicokinetics. *Food Chem Toxicol* 2006; **44**: 462–475.

16 Born, SL, Hu, JK, Lehman-McKeeman, LD. o-hydroxyphenylacetaldehyde is a hepatotoxic metabolite of coumarin. *Drug Metab Dispos* 2000a; **28**: 218–223.

17 Born, SL, Caudill, D, Smith, BJ, Lehman-McKeeman, LD. In vitro kinetics of coumarin 3,4-epoxidation: application to species differences in toxicity and carcinogenicity. *Toxicol Sci* 2000b; **58**: 23–31.

Available online at www.sciencedirect.com
ScienceDirect
Toxicology and Applied Pharmacology 229 (2008) 290–299
Toxicology and Applied Pharmacology
www.elsevier.com/locate/ytaap

Gene expression profiling in rat liver treated with compounds inducing phospholipidosis

Mitsuhiro Hirode [a,b], Atsushi Ono [b,c], Toshikazu Miyagishima [b], Taku Nagao [d], Yasuo Ohno [c], Tetsuro Urushidani [b,e,*]

[a] Development Research Center, Pharmaceutical Research Division, Takeda Pharmaceutical Company Limited, Yodogawa-ku, Osaka, 532-8686, Japan
[b] Toxicogenomics Project, National Institute of Biomedical Innovation, Ibaraki, Osaka, 567-0085, Japan
[c] National Institute of Health Sciences, Setagaya-ku, Tokyo 158-8501, Japan
[d] Food Safety Commission of Japan, Chiyoda-ku, Tokyo, 100-8989, Japan
[e] Department of Pathophysiology, Doshisha Women's College of Liberal Arts, Kyotanabe, Kyoto 610-0395, Japan

Received 27 October 2007; revised 14 January 2008; accepted 19 January 2008
Available online 14 February 2008

Abstract

We have constructed a large-scale transcriptome database of rat liver treated with various drugs. In an effort to identify a biomarker for diagnosis of hepatic phospholipidosis, we extracted 78 probe sets of rat hepatic genes from data of 5 drugs, amiodarone, amitriptyline, clomipramine, imipramine, and ketoconazole, which actually induced this phenotype. Principal component analysis (PCA) using these probes clearly separated dose- and time-dependent clusters of treated groups from their controls. Moreover, 6 drugs (chloramphenicol, chlorpromazine, gentamicin, perhexiline, promethazine, and tamoxifen), which were reported to cause phospholipidosis but judged as negative by histopathological examination, were designated as positive by PCA using these probe sets. Eight drugs (carbon tetrachloride, coumarin, tetracycline, metformin, hydroxyzine, diltiazem, 2-bromoethylamine, and ethionamide), which showed phospholipidosis-like vacuolar formation in the histopathology, could be distinguished from the typical drugs causing phospholipidosis. Moreover, the possible induction of phospholipidosis was predictable by the expression of these genes 24 h after single administration in some of the drugs. We conclude that these identified 78 probe sets could be useful for diagnosis of phospholipidosis, and that toxicogenomics would be a promising approach for prediction of this type of toxicity.

Keywords: Phospholipidosis; Toxicogenomics; Rat; Liver; Principal component analysis

Introduction

The toxicogenomics project was a 5-year collaborative project by the National Institute of Biomedical Innovation (NIBIO), the National Institute of Health Science (NIHS), and 15 pharmaceutical companies in Japan that started in 2002 (Urushidani and Nagao, 2005). Its aim was to construct a large-scale toxicology database of transcriptome for prediction of toxicity of new chemical entities in the early stage of drug development. About 150 chemicals, mainly medicinal compounds, were selected, and gene expression in liver (also kidney in some cases) was comprehensively analyzed by using Affymetrix GeneChip®. In 2007, the project was finished and the whole system, consisting of the database, the analyzing system and the prediction system, was completed and named as TG-GATEs (Genomics Assisted Toxicity Evaluation System developed by the Toxicogenomics Project, Japan). The present mission is to identify potential biomarker gene lists useful for prediction or diagnosis of drug-induced hepato- and nephro-toxicity using this system.

In toxicity studies, phospholipidosis (PLsis) is often observed in various tissues including liver, kidney, and lung. PLsis is a lipid storage disease characterized by intracellular accumulation of phospholipids and the appearance of membranous lamellar inclusions known as lamellar bodies. Its pathogenesis has been thought to be the unbalance of phospholipid turnover. As for drug-induced PLsis, it is well known that cationic

* Corresponding author. Department of Pathophysiology, Doshisha Women's College of Liberal Arts, Kyotanabe, Kyoto 610-0395, Japan. Fax: +81 774 65 8689.
E-mail address: turushid@dwc.doshisha.ac.jp (T. Urushidani).

0041-008X/$ - see front matter © 2008 Elsevier Inc. All rights reserved.
doi:10.1016/j.taap.2008.01.036

amphiphilic drugs (CADs), characterized by a hydrophobic ring structure and a hydrophilic side chain with a charged amine group have the potential to cause PLsis. Therefore, it has been postulated that drug-induced PLsis involves direct binding of CADs to phospholipids, subsequently creating a complex that is resistant to degradation by phospholipases (Reasor et al., 2006). There is also an observation that some CADs can cause PLsis by directly inhibiting phospholipase activity (Halliwell, 1997; Reasor et al., 2006). Although much effort has been done to establish the methods to predict PLsis of drugs (Tomizawa et al., 2006), sensitive diagnostic markers and effective prognostic markers are still desired.

In the present study, we selected PLsis in liver as a target phenotype, and tried to identify candidate biomarkers that enable the cell to discriminate chemicals with the potential to cause this phenotype for application of TG-GATEs.

Materials and methods

Compounds. Compounds used for the data analysis are listed in Table 1, in which the chemical name, abbreviation, dosage, administration route and vehicle used in the study are summarized.

Animal treatment. The experiments were carried out as previously described in the literature (Takashima et al., 2006). Male Crl:CD(SD) rats were purchased from Charles River Japan Inc., (Kanagawa, Japan) at 5-weeks of age. After a 7-day quarantine and acclimatization period, the animals were divided into groups of 5 animals using a computerized stratified random grouping method based on body weight for each age. The animals were individually housed in stainless-steel cages in a room that was lighted for 12 h (7:00–19:00) daily, ventilated with an air-exchange rate of 15 times per hour, and maintained at 21–25 °C with a relative humidity of 40–70%. Each animal was allowed free access to water and pellet food (CRF-1, sterilized by radiation, Oriental Yeast Co., Japan). Rats in each group were orally administered with various drugs suspended or dissolved either in 0.5% methylcellulose solution (MC) or corn oil according to their dispersibility, except for gentamicin and 2-bromoethylamine, which were dissolved in saline and administered intravenously. The animals were treated for 3, 7, 14 or 28 days and sacrificed 24 h after the last dosing. Blood samples were collected to a heparinized tube under ether anesthesia from the abdominal aorta after which the animals were euthanized.

The experimental protocols were reviewed and approved by the Ethics Review Committee for Animal Experimentation of the National Institute of Health Sciences.

Microarray analysis. After collecting the blood, the animals were euthanized by exsanguination from the abdominal aorta under ether anesthesia. An aliquot of the sample (about 30 mg) for RNA analysis was obtained from the left lateral lobe of the liver in each animal immediately after termination, kept in RNAlater® (Ambion, Austin, TX, USA) overnight at 4 °C, and then frozen at −80 °C until use. Liver samples were homogenized with the buffer RLT supplied in RNeasy Mini Kit (Qiagen, Valencia, CA, USA), and total RNA was isolated according to the manufacturer's instructions. Microarray analysis was conducted on 3 out of 5 samples for each group by using GeneChip® Rat Genome 230 2.0 Arrays (Affymetrix, Santa Clara, CA, USA), containing 31,042 probe sets. The procedure was conducted basically according to the manufacturer's instructions using Superscript Choice System (Invitrogen, Carlsbad, CA, USA) and T7-(dT)24-oligonucleotide primer (Affymetrix) for cDNA synthesis, cDNA Cleanup Module (Affymetrix) for purification, and BioArray High yield RNA Transcript Labeling Kit (Enzo Diagnostics, Farmingdale, NY, USA) for synthesis of biotin-labeled cRNA. Ten micrograms of fragmented cRNA was hybridized to a Rat Genome 230 2.0 Array for 18 h at 45 °C at 60 rpm, after which the array was washed and stained by streptavidin–phycoerythrin using Fluidics Station 400 (Affymetrix) and scanned by Gene Array Scanner (Affymetrix). The digital image files were processed by Affymetrix Microarray Suite version 5.0. Microarray image data were analyzed with GeneChip Operating Software (Affymetrix).

The digital image files were processed by Affymetrix Microarray Suite version 5.0 and the intensities were normalized for each chip by setting the mean intensity to 500 (per chip normalization).

Statistical analysis. In order to extract probe sets related to PLsis, we first employed gene expression data of rat liver treated with repeated administration for 3, 7, 14, and 28 days of AM, AMT, CPM, IMI and KC in our database, and they are known to cause PLsis, and in fact, the induction of this disease was confirmed in the present study.

After removing the probe sets with Affymetrix absent call in the whole 48 sample set ($N=3$ for 4 time points and 4 dose levels for one drug), differentially

Table 1
Compounds

Compound name	Abbreviation	Dose (dose level, mg/kg)			Administration route	Vehicle
		Low	Middle	High		
Amiodarone	AM	200/20*	600/60*	2000/200*	PO	MC
Amitriptyline	AMT	15	50	150	PO	MC
Clomipramine	CPM	10	30	100	PO	MC
Imipramine	IMI	10	30	100	PO	MC
Ketoconazole	KC	10	30	100	PO	MC
Chloramphenicol	CMP	100	300	1000	PO	MC
Chlorpromazine	CPZ	4.5	45/15*	150/45*	PO	MC
Gentamicin	GMC	10	30	100	IV	SA
Perhexiline	PH	15	50	150	PO	MC
Promethazine	PMZ	20	60	200	PO	MC
Tamoxifen	TMX	6	20	60	PO	CO
Carbon tetrachloride	CCl4	30	100	300	PO	CO
Coumarin	CMA	15	50	150	PO	CO
Tetracycline	TC	100	300	1000	PO	MC
Metformin	MFM	100	300	1000	PO	MC
Hydroxyzine	HYZ	10	30	100	PO	MC
Diltiazem	DIL	80	240	800	PO	MC
2-bromoethylamine	BEA	6/2*	20/6*	60/20*	IV	SA
Ethionamide	ETH	100/30*	300/100*	1000/300*	PO	MC

*: as single dose/repeated dose.
PO: peroral, IV: intravenous.
MC: 0.5 w/v% methylcellulose; SA: saline; CO: corn oil.

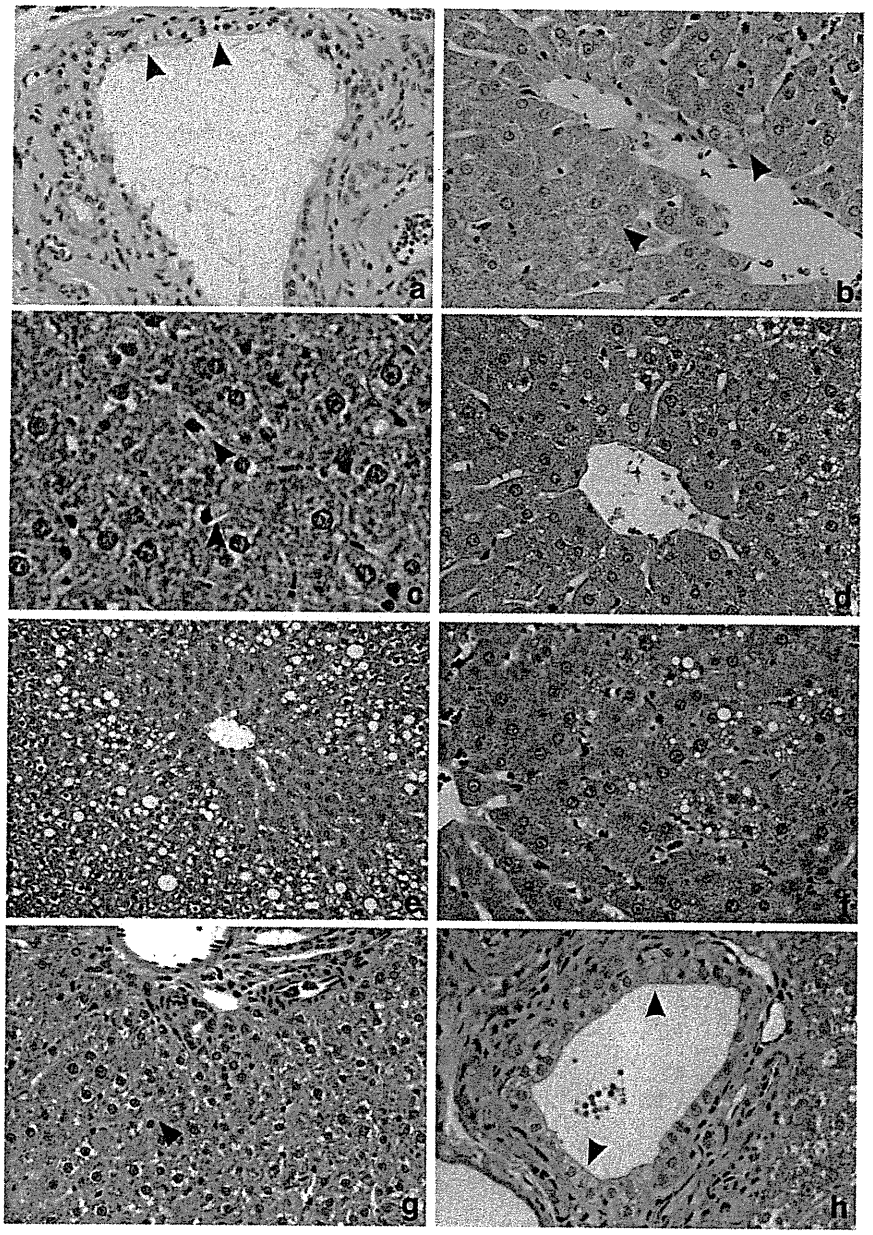

Fig. 1. Histopathology of rat liver treated with amiodarone, amitriptyline, clomipramine, imipramine, and ketoconazole. a–c. Amiodarone 200 mg/kg, 29th day. Vacuolations in the bile duct cell (a) in the hepatocyte (b) and in the Kupffer cell (c) are evident (arrowheads). d. Amitriptyline 150 mg/kg, 29th day. Vacuolation in the hepatocyte is evident. e. Clomipramine 100 mg/kg, 29th day. Vacuolation is noted in the midlobular hepatocytes. f–g. Imipramine 100 mg/kg, 29th day. Vacuolations in the hepatocyte (f) and in the Kupffer cell (g) are evident. h. Ketoconazole 100 mg/kg, 29th day. Vacuolation occurs exclusively in the bile duct (arrowheads).

expressed genes by the treatment were extracted by Welch's ANOVA ($p<0.05$) for the dose level at any time point. This procedure was continued for 4 time points and genes showing significant change, and any points were combined as PLsis responsive genes. In the next step, commonly mobilized genes among these 5 chemicals were selected.

Principal component analysis (PCA) of the GeneChip data was also performed using Spotfire DecisionSite.

Pathway and gene ontology (GO) analysis. The identified probe sets were subjected to analysis of Kyoto Encyclopedia of Genes and Genomes (KEGG) pathway and GO analysis by DAVID (Database for Annotation, Visualization, and Integrated Discovery; http://apps1.niaid.nih.gov/david/ using Fisher's exact test (Dennis et al., 2003). Level 5 analysis was adopted.

Results

Histopathological examination

The results of histopathological examination of 5 compounds (AM, AMT, CPM, IMI and KC) known to induce PLsis are shown in Fig. 1 and Table 2. For most cases, clear vacuolization was observed in the cytoplasm of hepatocytes, and this change tended to progress with dose and time. Vacuolation was also noted in Kupffer cell (AM, IMI) or bile duct (AM). In the case of KC, vacuolation occurred exclusively in the bile duct.

Table 2
Histopathological findings

Compound	Findings	Time	Dose		
			Low	Middle	High
AM	Vacuolization, bile duct cell	3 h–4 day	–	–	–
		8 day	–	–	3/5(±)
		15 day	–	–	1/5(±), 4/5(+)
		29 day	–	–	4/4(+)
	Vacuolization, hepatocyte	3 h–8 day	–	–	–
		15 day	–	–	2/5(±)
		29 day	–	–	4/4(±)
	Vacuolization, Kupffer cell	3 h–8 day	–	–	–
		15 day	–	–	5/5(±)
		29 day	–	–	4/4(±)
AMT	Vacuolization, hepatocyte	3 h–4 day	–	–	–
		8 day	–	–	4/5(±)
		15 day	–	1/5(±)	5/5(+)
		29 day	–	1/5(±), 2/5(+)	1/3(+), 2/3(2+)
CPM	Vacuolization, hepatocyte	3 h–15 day	–	–	–
		29 day	–	–	1/5(±), 1/5(+)
IMI	Vacuolization, hepatocyte	3 h–4 day	–	–	–
		8 day	–	–	4/5(±)
		15 day	–	–	1/5(±), 2/5(+)
		29 day	–	2/5(±)	1/4(±), 3/4(+)
	Vacuolization, Kupffer cell	3 h–8 day	–	–	–
		15 day	–	–	3/5(±)
		29 day	–	–	–
KC	Vacuolization, bile duct cell	3 h–24 h	–	–	–
		4 day	–	–	5/5(+)
		8 day	–	–	5/5(+)
		15 day	–	1/5(+)	2/5(+), 3/5(2+)
		29 day	–	1/5(±), 4/5(+)	5/5(2+)
CMP	Abnormality	3 h–29 day	–	–	–
CPZ	Abnormality	3 h–29 day	–	–	–
GMC	Abnormality	3 h–29 day	–	–	–
PH	Abnormality	3 h–29 day	–	–	–
PMZ	Abnormality	3 h–29 day	–	–	–
TMX	Abnormality	3 h–29 day	–	–	–
CCl4	Degeneration, fatty, hepatocyte	3 h–9 h	–	–	–
		24 h	–	2/5(±)	1/5(±), 4/5(+)
		4 day	4/5(±), 1/5(+)	5/5(+)	1/5(±), 4/5(+)
		8 day	1/5(±), 4/5(+)	5/5(+)	4/5(+), 1/5(2+)
		15 day	1/5(±), 4/5(+)	5/5(+)	4/5(+), 1/5(2+)
		29 day	5/5(+)	4/5(+), 1/5(2+)	2/5(+), 2/5(2+), 1/5(3+)
CMA	Vacuolization, hepatocyte	3 h–8 day	–	–	–
		15 day	–	–	2/5(±), 1/5(+)
		29 day	–	–	5/5(+)
TC	Vacuolization, hepatocyte	3 h–8 day	–	–	–
		15 day	–	–	2/5(±)
		29 day	–	–	2/5(±)
MFM	Deposit, glycogen, hepatocyte	3 h–24 h	–	–	–
		4 day	–	2/5(±)	5/5(±)
		8 day	–	–	2/5(±)
		15 day	–	–	2/5(±)
		29 day	–	–	1/5(±)
HYZ	Vacuolization, hepatocyte	3 h–8 day	–	–	–
		15 day	–	–	2/5(±), 2/5(+)
		29 day	–	–	4/5(+), 1/5(2+)
DIL	Vacuolization, hepatocyte	3 h–4 day	–	–	–
		8 day	–	–	2/5(±)
		15 day	–	1/5(±)	5/5(±)
		29 day	–	4/5(±)	4/4(±)
BEA	Vacuolization, hepatocyte	3 h–8 day	–	–	–
		15 day	–	–	2/5(+)
		29 day	–	4/5(+)	4/5(+)
ETH	Vacuolization, hepatocyte	3 h–24 h	–	–	–
		4 day	–	4/5(+), 1/5(2+)	5/5(+)
		8 day	–	3/5(±), 2/5(+)	3/3(+)
		15 day	–	2/5(±), 3/5(+)	2/5(±), 3/5(+)
		29 day	–	2/5(+)	NA

–: not remarkable, ±: minimal, +: mild, 2+: moderate, 3+: severe, NA: not applicable.

Microarray data analysis

Differentially expressed genes with statistical significance were extracted from each of 5 representative drugs inducing PLsis, as described in the Materials and methods section. The numbers of extracted probe sets were 4915 for AM, 3565 for AMT, 1907 for CPM, 2339 for IMI, and 3482 for KC. We then selected the probe sets that were commonly changed in all compounds and 78 probe sets were obtained. The list of these probe sets is shown in Table 3. Based on gene ontology, the contents of genes related to carboxylic acid metabolism, electron transport, amino acid metabolism, amine catabolism, and nitrogen compound catabolism were significantly high (Table 4). Although not significant, 4 lipid biosynthesis-related genes were contained. This feature might reflect the cellular changes related to lipid metabolism in association with PLsis.

Principal component analysis (PCA)

Using the 78 probe sets extracted as above, PCA was performed on the 5 drugs inducing PLsis. As shown in Fig. 2,

Table 3
List of 78 probe sets changed in 5 compounds inducing PLsis

Probe set ID	Gene title	Gene symbol
1367676_at	High mobility group box 2	Hmgb2
1367819_at	Glutamate oxaloacetate transaminase 2, mitochondrial	Got2
1368016_at	Peroxisomal *trans*-2-enoyl-CoA reductase	Pecr
1368171_at	Lysyl oxidase	Lox
1368213_at	P450 (cytochrome) oxidoreductase	Por
1368275_at	Sterol-C4-methyl oxidase-like	Sc4mol
1368403_at	Retinoblastoma-like 2	Rbl2
1368467_at	Cytochrome P450, family 4, subfamily F, polypeptide 2	Cyp4f2
1368520_at	Apolipoprotein A-IV	Apoa4
1368618_at	Growth factor receptor bound protein 14	Grb14
1368718_at	Aldehyde dehydrogenase family 1, subfamily A4	Aldh1a4
1368778_at	Solute carrier family 6 (neurotransmitter transporter, taurine), member 6	Slc6a6
1368905_at	Carboxylesterase 2 (intestine, liver)	Ces2
1368931_at	SH3-domain GRB2-like 3	Sh3gl3
1368977_a_at	Fractured callus expressed transcript 1	Fxc1
1369275_s_at	Cytochrome P450 IIA1 (hepatic steroid hydroxylase IIA1) gene	Cyp2a1
1369737_at	cAMP responsive element modulator	Crem
1369850_at	UDP-glucuronosyltransferase 2 family, polypeptide A1	Ugt2a1
1370004_at	H2A histone family, member Y	H2afy
1370054_at	Cyclin-dependent kinase inhibitor 2C (p18, inhibits CDK4)	Cdkn2c
1370375_at	Glutaminase 2 (liver, mitochondrial)	Gls2
1370583_s_at	ATP-binding cassette, subfamily B (MDR/TAP), member 1	Abcb1
1370613_s_at	UDP glycosyltransferase 1 family, polypeptide A1	Ugt1a1
1370698_at	Liver UDP-glucuronosyltransferase, phenobarbital-inducible form liver	Udpgtr2
1371076_at	Cytochrome P450, family 2, subfamily b, polypeptide 15	Cyp2b15
1371089_at	Transcribed locus	–
1371412_a_at	Neuronal regeneration related protein	Nrep
1371546_at	Similar to TR4 orphan receptor-associated protein TRA16	LOC361128
1371680_at	Similar to gamma-aminobutyric acid (GABA(A)) receptor-associated protein-like 1	LOC683917
1371809_at	Mitochondrial ribosomal protein S18B	Mrps18b
1371875_at	Mannosidase, beta A, lysosomal	Manba
1372056_at	CKLF-like MARVEL transmembrane domain containing 6	Cmtm6
1372124_at	Eukaryotic translation initiation factor 4B	Eif4b
1372181_at	Similar to expressed sequence AA408877	RGD1308513
1372479_at	Transcribed locus, moderately similar to NP_064456.1 fibrinogen, beta polypeptide [*Rattus norvegicus*]	–
1372602_at	Similar to genethonin 1	RGD1311800
1372885_at	Transcribed locus	–
1373015_at	Ring finger protein 11 (predicted)	Rnf11_predicted
1373626_at	Transcribed locus	–
1373823_at	Similar to cyclin-dependent kinases regulatory subunit 2 (CKS-2) (predicted)	RGD1562047_predicted
1373924_at	Similar to C530044N13Rik protein	RGD1306568
1373970_at	Similar to RIKEN cDNA 9230117N10	RGD1311155
1374531_at	Transcribed locus	–
1374953_at	Similar to CG12279-PA	LOC500420
1375423_at	MAX-like protein X	Mlx
1375637_at	Similar to RIKEN cDNA 1110003E01	RGD1311122
1375909_at	Similar to glutathione transferase GSTM7-7	MGC108896
1377019_at	Transcribed locus	–
1378016_at	Echinoderm microtubule associated protein-like 4 (predicted)	Eml4_predicted
1380254_at	Transcribed locus, moderately similar to NP_079928.1 general transcription factor III A [*Mus musculus*]	–
1384169_a_at	Vav2 oncogene (predicted)	Vav2_predicted
1386857_at	Stathmin 1	Stmn1
1386917_at	Pyruvate carboxylase	Pc
1387006_at	Rat senescence marker protein 2A gene, exons 1 and 2	Smp2a
1387022_at	Aldehyde dehydrogenase family 1, member A1	Aldh1a1
1387031_at	Endoplasmic reticulum protein 29	Erp29
1387093_at	Solute carrier organic anion transporter family, member 1a4	Slco1a4
1387094_at	Solute carrier organic anion transporter family, member 1a4	Slco1a4
1387109_at	P450 (cytochrome) oxidoreductase	Por
1387118_at	Cytochrome P450, family 3, subfamily a, polypeptide 1	Cyp3a1
1387203_at	Glucokinase regulatory protein	Gckr
1387223_at	Aminoadipate aminotransferase	Aadat

Table 3 (*continued*)

Probe set ID	Gene title	Gene symbol
1387307_at	Histidine ammonia lyase	Hal
1387511_at	Cytochrome P450 IIA1 (hepatic steroid hydroxylase IIA1) gene	Cyp2a1
1387665_at	Betaine-homocysteine methyltransferase	Bhmt
1387669_a_at	Epoxide hydrolase 1, microsomal	Ephx1
1387759_s_at	UDP glycosyltransferase 1 family, polypeptide A1	Ugt1a1
1387793_at	Transcribed locus, strongly similar to NP_075738.1 yippee-like 1 [*Mus musculus*]	–
1388212_a_at	RT1 class Ib, locus S3	RT1-S3
1388348_at	Transcribed locus	–
1388425_at	Similar to RIKEN cDNA D130038B21	RGD1305890
1388874_at	Metastasis suppressor 1 (predicted)	Mtss1_predicted
1389319_at	Similar to endoplasmic reticulum-Golgi intermediate compartment protein 1 (ER-Golgi intermediate compartment 32 kDa protein) (ERGIC-32)	LOC287177
1389557_at	Testis expressed gene 261	Tex261
1389986_at	CDNA clone IMAGE:7321089	–
1390455_at	Abhydrolase domain containing 2 (predicted)	Abhd2_predicted
1398754_at	Ubiquitin A-52 residue ribosomal protein fusion product 1	Uba52
1398848_at	Suppression of tumorigenicity 13	St13

treated samples were dose-dependently separated to form clusters from controls, mainly toward the direction of PC1 (contribution rate: 34.8%). In order to examine the time-dependency, all the samples were aligned on a one dimensional graph of PC1 (Fig. 3). It appears that the PC1 value generally increased with time as well as with a dose of these drugs. In case of KC, time- and dose-dependency were obscure, although the treated group clearly formed a cluster separated from the control cluster. Of the genes contributing to PC1, those with high eigenvector value were listed in Table 5. We noticed that the top 4 genes are cytochrome oxidoreductase, sterol-C4-methy oxidase-like, aldehyde dehydrogenase 1A4, and carboxylesterase 2, which are all involved in lipid metabolism.

Distinction of 6 compounds reported to induce PLsis with no abnormality in present histopathological examination

In a survey of the literature, in addition to the 5 drugs above, 6 more drugs, i.e., CMP, CPZ, GMC, PH, PMZ, and TMX in our database, are reported to induce PLsis, but no such histopathological abnormalities were confirmed in the present examination. We then applied PCA using the 78 probe sets on these 6 drugs and we show the results in Fig. 4 as a one dimensional graph with PC1. It was revealed that these 6 drugs were also separated from control clusters the same way as the 5 typical drugs inducing PLsis. Of these, some drugs such as CPZ, GMC and PH, did not change their position very much, but their extent was roughly equivalent to that of KC.

Table 4
GO analysis of identified 78 probe sets

Term	Count	Percent	*P*-value
Carboxylic acid metabolism	10	11.5	1.90E–04
Electron transport	6	6.9	1.20E–02
Amino acid metabolism	5	5.7	1.80E–02
Amine catabolism	3	3.4	3.20E–02
Nitrogen compound catabolism	3	3.4	3.40E–02
Lipid biosynthesis	4	4.6	6.10E–02

Distinction of 8 compounds showing pathological changes similar to PLsis

When examination by light microscope of HE-stained specimens is performed, we sometimes encounter a phenotype (not PLsis but another pathological change), such as lipidosis, deposition of glycogen, or hydropic degeneration, and they are quite difficult to distinguish from each other. In our database, we identified 8 drugs (CCL4, CMA, TC, MFM, HYZ, DIL, BEA, and ETH) showing such pathological changes in liver. The histopathological description of each was as follows: CCL4: "degeneration, fatty, hepatocyte"; CMA, TC, HYZ, DIL, BEA, ETH: "vacuolization, hepatocyte"; and MFM: "deposit, glycogen, hepatocyte". To examine the efficiency of the 78 probe sets, PCA was applied to these 8 pseudo-positive compounds.

As shown in Fig. 5, most of the treated samples stayed in the position close to that of the control samples. Exceptionally, HYZ and DIL formed separate clusters from the controls, as 5 standard compounds inducing PLsis.

Possible distinction of the samples 24 h after a one time dosage

The above results clearly suggested that the list of extracted 78 probe sets was a useful diagnostic marker for PLsis in rat liver. The next question is whether the list works as a prognostic marker for PLsis. To examine this possibility, we performed PCA using the list for the gene expression profile 24 h after the single dose, and practically no pathological changes had occurred at that time. As shown in Fig. 6 left, AM 20, 60, and 200 mg/kg had a high PC1 value in repeated administration for 3 days or more, whereas that in the single dose group was close to the cluster of the control group. Then we additionally performed single dose experiments using higher doses, i.e., 200,

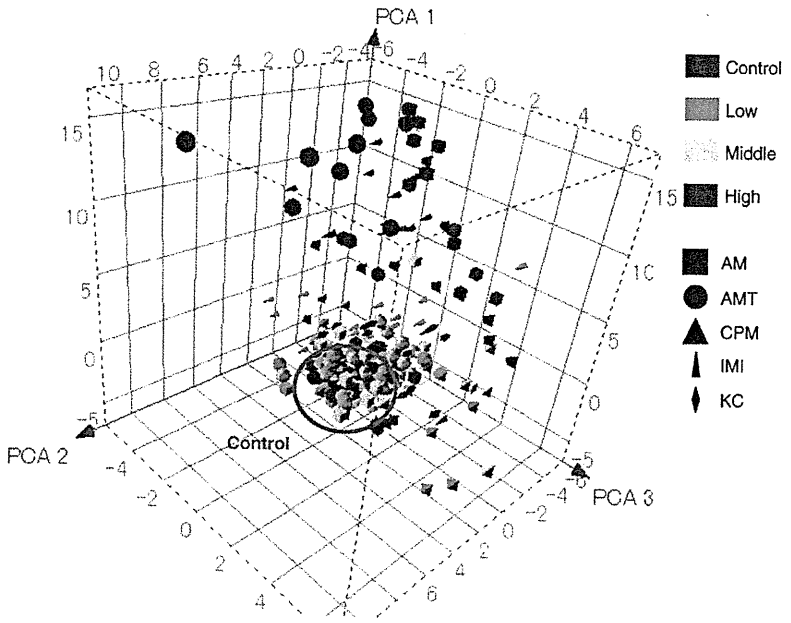

Fig. 2. Principal component analysis of gene expression profiles of amiodarone (AM), amitriptyline (AMT), clomipramine (CPM), imipramine (IMI), and ketoconazole (KC) that induced phospholipidosis in liver in the present study using the commonly mobilized 78 probe sets. Results are expressed as a three dimensional figure with PC1, 2, and 3. Treated samples were dose-dependently separated from the cluster of controls (circled by a blue line), mainly toward the direction of PC1 (contribution rate: 34.8%). For simplicity, rats receiving the same dose with different durations (3, 7, 14 and 28 days, N=3 for each; 12 total) were expressed by the same symbol.

600, and 2000 mg/kg of AM (Fig. 6, right). It was revealed that the group receiving a single dose of 2000 mg/kg AM clustered at a position clearly higher than controls with equivalent PCA1 values receiving a repeated dose of 200 mg/kg for 3 days. In the case of CPZ, the samples at 24 h after the 45 mg/kg single dosing were clearly separated from control samples to an extent more than that of the repeated dose samples (Fig. 7). We then performed additional single dose experiments using 45 and 150 mg/kg CPZ. It was clear from Fig. 7 that 150 mg/kg CPZ showed a higher PC1 value than the 45 mg/kg group.

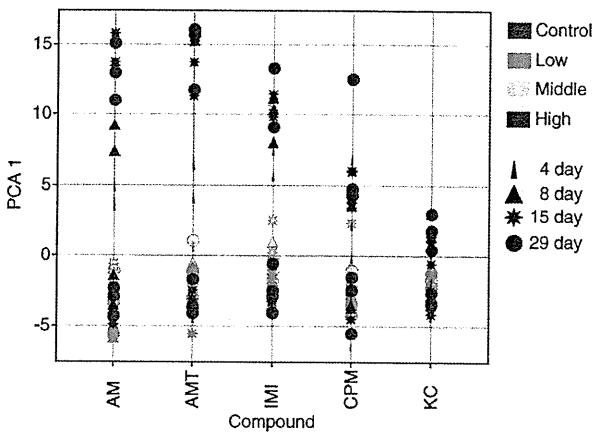

Fig. 3. Principal component analysis the same as Fig. 2 but with one dimensional expression using principal component 1. For each drug, each individual rat is depicted by a symbol with a different color and shape as shown on the right panel.

Discussion

PLsis has been one of the main concerns in the course of drug development, since its appropriate biomarkers are lacking, especially in the clinical field. In order to assess PLsis, a variety of in vitro methodologies have recently been described, e.g., using fluorescent dyes (Casartelli et al., 2003) or fluorescently labeled phospholipids (Kasahara et al., 2006, Nioi et al., 2007) in cell culture. However, these assay systems only work to estimate the potential of PLsis, but not to tell its mechanism and thus they do not help in deciding whether to go ahead or to switch to other candidates in the development process. One promising strategy would be a toxicogenomics approach. Sawada et al. (2005) recently identified a panel of 17 genes where the expression profile would predict the possibility of PLsis using HepG2 cells. This result was further transferred to a 96-well plate to attain a high throughput genomics-based platform (Sawada et al., 2006). Although the advantage of the genomics-based strategy was postulated to elucidate the background toxicological mechanism, the gene expression changes have not been related to the pathophysiological aspects of PLsis. It has been suggested that PLsis is induced by the disturbance of lipid turnover, i.e., excess of lipid biosynthesis, inhibition of lipid degradation enzymes (especially lysosomal phospholipase A2), and inhibition of lipid transporter in lysosomes. In the case of drug-induced PLsis, most of it has been attributed to the inhibition of phospholipase

Table 5
List of 28 probe sets contributing PC1

Ranking	Probe set ID	Gene title	Eigenvalue
1	1368905_at	Carboxylesterase 2 (intestine, liver)	0.165043
2	1387759_s_at	UDP glycosyltransferase 1 family, polypeptide A1	0.163056
3	1387022_at	Aldehyde dehydrogenase family 1, member A1	0.158847
4	1371076_at	Cytochrome P450, family 2, subfamily b, polypeptide 15	0.156238
5	1387118_at	Cytochrome P450, family 3, subfamily a, polypeptide 1	0.153634
6	1387109_at	P450 (cytochrome) oxidoreductase	0.152900
7	1371089_at	Transcribed locus	0.152322
8	1368718_at	Aldehyde dehydrogenase family 1, subfamily A4	0.147161
9	1370613_s_at	UDP glycosyltransferase 1 family, polypeptide A1	0.145621
10	1368977_a_at	Fractured callus expressed transcript 1	0.145613
11	1370583_s_at	ATP-binding cassette, subfamily B (MDR/TAP), member 1	0.145395
12	1380254_at	Transcribed locus, moderately similar to NP_079928.1 general transcription factor III A [*Mus musculus*]	0.145244
13	1387669_a_at	Epoxide hydrolase 1, microsomal	0.144549
14	1370698_at	Liver UDP-glucuronosyltransferase, phenobarbital-inducible form liver	0.143250
15	1368213_at	P450 (cytochrome) oxidoreductase	0.142376
16	1375423_at	MAX-like protein X	0.135972
17	1387094_at	Solute carrier organic anion transporter family, member 1a4	0.131073
18	1372602_at	Similar to genethonin 1	0.129514
19	1369850_at	UDP-glucuronosyltransferase 2 family, polypeptide A1	0.129217
20	1368275_at	Sterol-C4-methyl oxidase-like	0.129122
21	1371875_at	Mannosidase, beta A, lysosomal	0.128496
22	1372479_at	Transcribed locus, moderately similar to NP_064456.1 fibrinogen, beta polypeptide [*Rattus norvegicus*]	0.127711
23	1387093_at	Solute carrier organic anion transporter family, member 1a4	0.127266
24	1371809_at	Mitochondrial ribosomal protein S18B	0.126952
25	1384169_a_at	Vav2 oncogene (predicted)	0.125901
26	1375909_at	Similar to glutathione transferase GSTM7-7	0.125538
27	1373924_at	Similar to C530044N13Rik protein	0.122349
28	1371680_at	Similar to gamma-aminobutyric acid (GABA(A)) receptor-associated protein-like 1	0.117093

activity either through the generation of CAD-phospholipid complexes or by direct inhibition of phospholipase activity (Reasor et al., 2006). It is clearly necessary to elucidate how these changes are reflected in gene expression in order to make a prediction based on the genomics approach.

In the present study, we extracted 78 genes commonly mobilized in the 5 typical PLsis-inducing drugs, i.e., AM (Honegger et al., 1993), AMT (Drenckhahn et al., 1976), CPM (Xia et al., 2000), IMI (Drew et al., 1981; Hansson et al., 1997) and KC (Whitehouse et al., 1994). By PCA, we used these genes to successfully separate the high risk group from the low risk ones, except for KC, which showed relatively obscure separation. This is reasonable, as the histopathology of KC only causes changes

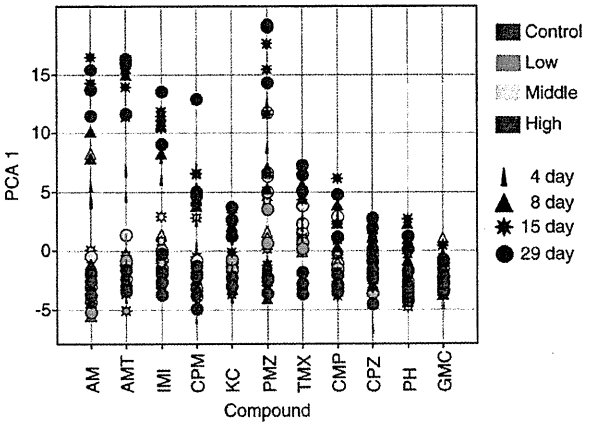

Fig. 4. Principal component analysis of gene expression profiles of 6 compounds reported to induce PLsis but no abnormality in present histopathological examination, i.e., chloramphenicol (CMP), chlorpromazine (CPZ), gentamicin (GMC), perhexiline (PH), promethazine (PMZ), and tamoxifen (TMX) using the commonly mobilized 78 probe sets. For comparison, 5 compounds shown in Figs. 2 and 3, amiodarone (AM), amitriptyline (AMT), clomipramine (CPM), imipramine (IMI), and ketoconazole (KC), are also included. Results are expressed as a one dimensional figure with PC1 (contribution rate: 34.8%). For each drug, each individual rat is depicted by a symbol with a different color and shape as shown on the right panel.

in the bile duct cells, in contrast to the other 4 drugs that elicit changes in the hepatocytes.

CMP (Joshi et al., 1989), CPZ (Kodavanti et al., 1990), GMC (Kacew, 1987), PH (Pessayre et al., 1979), PMZ (Joshi et al., 1989) and TMX (Reasor and Kacew, 2001) have also been reported to induce PLsis, but we could not detect PLsis in liver by histopathological examinations in the present study. This is not surprising when the sensitivity of detection by histopathology is

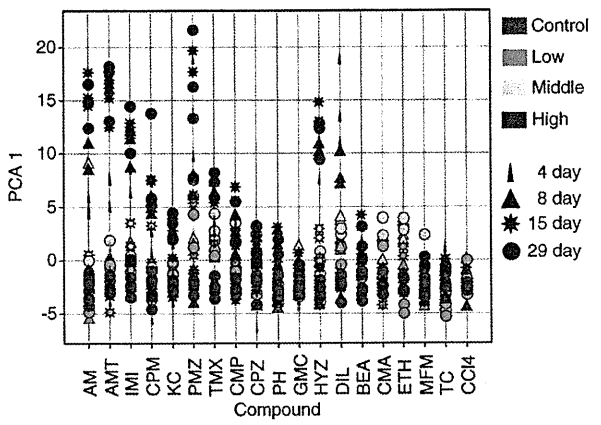

Fig. 5. Principal component analysis of gene expression profiles of 8 compounds showing pathological changes similar to PLsis, i.e., carbon tetrachloride (CCL4), coumarin (CMA), tetracycline (TC), metformin (MFM), hydroxyzine (HYZ), diltiazem (DIL), 2-bromoethylamine (BEA), and ethionamide (ETH), using the commonly mobilized 78 probe sets. For comparison, the 5 compounds shown in Figs. 2 and 3, amiodarone (AM), amitriptyline (AMT), clomipramine (CPM), imipramine (IMI) and ketoconazole (KC), and the 6 compounds in Fig. 4, chloramphenicol (CMP), chlorpromazine (CPZ), gentamicin (GMC), perhexiline (PH), promethazine (PMZ), and tamoxifen (TMX) are also included. Results are expressed as a one dimensional figure with PC1 (contribution rate: 34.8%). For each drug, each individual rat is depicted by a symbol with a different color and shape as shown on the right panel.

considered. In particular, our dose setting for the database was based on preliminary experiments of repeated dosing for 7 days with the proviso that all animals are to survive for 28 days. This sometimes brings about a situation that the dose level is too low for certain phenotypes. This point is particularly problematic when biomarker gene lists are to be extracted based on the actually observed phenotype. Of these 6 drugs, we could judge CMP, PMZ and TMX as positive by PCA using the present marker genes, whereas CPZ, GMC and PH were weakly positive or almost negative. These observations could be due to a feature of the marker genes: a considerable part of them actually reflects the occurring pathological changes, namely, they work as diagnostic markers. The fact that some of the drugs could be judged as positive suggested that their diagnosis from marker genes was more sensitive than pathological examination.

GMC has been reported to cause PLsis in kidney tissue and this is associated with renal tubular toxicity (Kaloyanides and Pastoriza-Munoz, 1980; Laurent et al., 1990). This might be attributed to its negative judgment for PLsis in liver since potential biochemical/pathological changes would mainly occur in kidney. It is of interest to investigate the gene expression changes in kidney, but another set of genes would be necessary to make a precise diagnosis for PLsis in kidney.

PH was selected as a PLsis-positive drug but appeared to be negative or a very weak positive in the present study using rats. This might be due to the species difference in the drug metabolism since the risk of PH-induced liver injury is higher in individuals with the P450IID6 poor-metabolizer phenotype (Morgan et al., 1984, Pessayre and Larrey, 1988).

Some compounds show morphological changes similar to PLsis. In our database, there are 8 such compounds, i.e., CCL4, CMA, TC, MFM, HYZ, DIL, BEA, and ETH. Of these, CCL4 (Weber et al., 2003), TC (Fréneaux et al., 1988), BEA (Thiele-

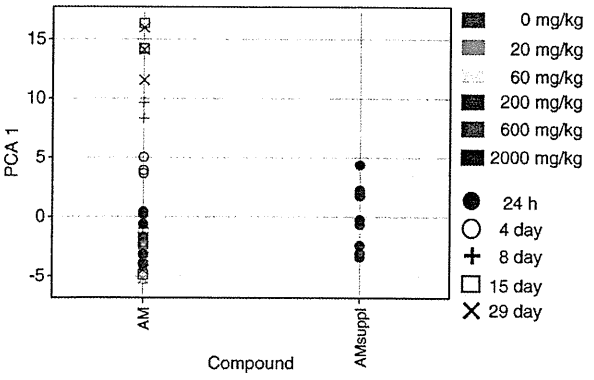

Fig. 6. Principal component analysis of gene expression profiles of amiodarone. Results are expressed as a one dimensional figure with PC1 (contribution rate: 34.8%). Each individual rat is depicted by a symbol with a different color and shape as shown on the right panel. On the left, the data of 24 h after a single treatment (filled symbols) are added to the data for repeated treatment (open or line symbols) shown in the previous figures. Note that the PC1 value of a single dose is low even at the highest dose, 200 mg/kg (red filled circle) compared with the repeated dose (red open or line symbols). On the left, a supplemental higher dose experiment was performed. Note that the higher dose (600 mg/kg, magenta; 2000 mg/kg, black) showed a dose-dependent increase in PC1 reaching to a value of 200 mg/kg at 4 days.

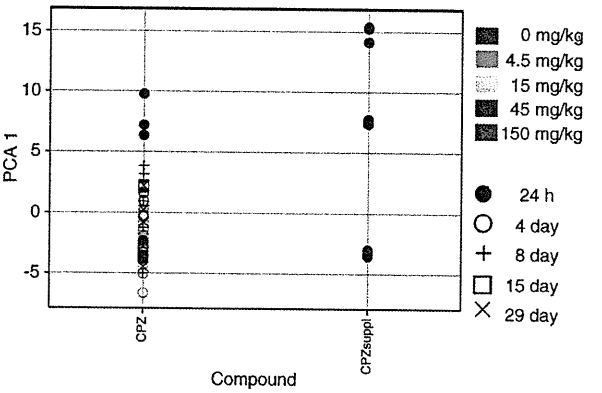

Fig. 7. Principal component analysis of gene expression profiles of chlorpromazine. Results are expressed as a one dimensional figure with PC1 (contribution rate: 34.8%). Each individual rat is depicted by a symbol with a different color and shape as shown on the right panel. On the left, the data of 24 h after a single treatment (filled symbols) are added to the data for repeated treatment (open or line symbols) shown in the previous figures. In contrast to the results in Fig. 6, the single dose of 45 mg/kg (red filled circle) gave higher PC1 values compared with samples of repeated dosing. On the left, a supplemental higher dose (150 mg/kg) experiment was performed in addition to 45 mg/kg. Note that the higher dose (magenta) showed even higher PC1 values.

mann et al., 1999), and ETH (Kuntz et al., 1968, Inouye et al., 1973) are reported to show morphology associated with a change in the lipid storage, i.e., lipidosis or steatosis. CMA is known to cause hepatic necrosis (Lake, 1984) and MFM induces a deposition of glycogen. These drugs, which do not induce PLsis, could be separated from the clusters of PLsis-inducing ones by PCA using the extracted genes. As for HYZ (Hruban et al., 1972), classified as PLsis-positive by PCA in this study, there is a recent report that it actually induced PLsis (Pelletier et al., 2007). The only exception was the case of DIL, which showed vacuolation in hepatocytes and was not considered as PLsis, but was classified as positive by PCA. Reviewing the PCA (Fig. 5) however, it is noticeable that the time-dependent changes in the PC1 value are exceptionally different from other drugs such that the value transiently increases with the peak at 4 days, then decreases with time and returns to negative at the 15th day. It is necessary to elucidate the mechanism of the unique change observed in DIL, but it appears that this drug is to be judged as pseudo-positive by the present criteria.

One important question is whether the toxicogenomics approach enables not only diagnosis but also prognosis of PLsis. The results shown in Figs. 6 and 7 provide a clue. In general, it appears to be difficult to predict the potential of PLsis occurring 14 days or later with repeated administration with the data for single dosing, but it could be possible when a high enough dose is applied in some cases. We are presently in a preliminary stage, but we hope to establish a really useful marker gene set in a future study with a strategic protocol, which can predict PLsis in liver by single dosing within 24 h. In the present study, we exclusively worked on liver where enough gene expression data are stored in our database. As PLsis occurs in organs other than liver, it is of interest to apply the present strategy to other organs such as kidney whose transcriptome data are now accumulating in our database.

There remain many problems to be solved in the present system, such as the improvement of accuracy and sensitivity, the elucidation of the functions of the genes in the list (especially in the pathological mechanism of PLsis), the breakthrough species difference, and so on. However, the presently identified 78 probe sets from gene expression data stored in TG-GATEs have provided a powerful starting tool.

Acknowledgment

This work was supported in part by the grants from Ministry of Health, Labour and Welfare of Japan, H14-001-Toxico.

References

Casartelli, A., Bonato, M., Cristofori, P., Crivellente, F., Dal Negro, G., Masotto, I., Mutinelli, C., Valko, K., Bonfante, V., 2003. A cell-based approach for the early assessment of the phospholipidogenic potential in pharmaceutical research and drug development. Cell Biol. Toxicol. 19, 161–176.

Dennis Jr., G., Sherman, B.T., Hosack, D.A., Yang, J., Gao, W., Lane, H.C., Lempicki, R.A., 2003. DAVID: database for annotation, visualization, and integrated discovery. Genome Biol. 4, P3.

Drenckhahn, D., Kleine, L., Lullmann-Rauch, R., 1976. Lysosomal alterations in cultured macrophages exposed to anorexigenic and psychotropic drugs. Lab. Invest. 35, 116–123.

Drew, R., Siddik, Z.H., Mimnaugh, E.G., Gram, T.E., 1981. Species and dose differences in the accumulation of imipramine by mammalian lungs. Drug Metab. Dispos. 9, 322–326.

Frénçaux, E., Labbe, G., Letteron, P., The Le Dinhi, Degott, C., Genève, J., Larrey, D., Pessayre, D., 1988. Inhibition of the mitochondrial oxidation of fatty acids by tetracycline in mice and in man: possible role in microvesicular steatosis induced by this antibiotic. Hepatology 8, 1056–1062.

Halliwell, W.H., 1997. Cationic amphiphilic drug-induced phospholipidosis. Toxicol. Pathol. 25, 53–60.

Hansson, A.L., Xia, Z., Berglund, M.C., Bergstrand, A., Depierre, J.W., Nässberger, L., 1997. Reduced cell survival and morphological alterations induced by three tricyclic antidepressants in human peripheral monocytes and lymphocytes and in cell lines derived from these cell types. Toxicol. In Vitro 11, 21–31.

Honegger, U.E., Zuehlke, R.D., Scuntaro, I., Schaefer, M.H., Toplak, H., Wiesmann, U.N., 1993. Cellular accumulation of amiodarone and desethylamiodarone in cultured human cells. Consequences of drug accumulation on cellular lipid metabolism and plasma membrane properties of chronically exposed cells. Biochem. Pharmacol. 45, 349–356.

Hruban, Z., Slesers, A., Hopkins, E., 1972. Drug-induced and naturally occurring myeloid bodies. Lab. Invest. 27, 62–70.

Inouye, B., Yoshimura, N., Wachi, T., 1973. Experimental studies on the mechanism of fatty liver formation induced by ethionamide. V. Liver and serum total cholesterol in ethionamide-administered rats. Kekkaku 48, 71–74.

Joshi, U.M., Rao, P., Kodavanti, S., Lockard, V.G., Mehendale, H.M., 1989. Fluorescence studies on binding of amphiphilic drugs to isolated lamellar bodies: relevance to phospholipidosis. Biochim. Biophys. Acta 1004, 309–320.

Kacew, S., 1987. Cationic amphiphilic drug-induced renal cortical lysosomal phospholipidosis: an in vivo comparative study with gentamicin and chlorphentermine. Toxicol. Appl. Pharmacol. 91, 469–746.

Kaloyanides, G.J., Pastoriza-Munoz, E., 1980. Aminoglycoside nephrotoxicity. Kidney Int, 18, 571–582.

Kasahara, T., Tomita, K., Murano, H., Harada, T., Tsubakimoto, K., Ogihara, T., Ohnishi, S., Kakinuma, C., 2006. Establishment of an in vitro high-throughput screening assay for detecting phospholipidosis-inducing potential. Toxicol. Sci. 90, 133–141.

Kodavanti, U.P., Lockard, V.G., Mehendale, H.M., 1990. In vivo toxicity and pulmonary effects of promazine and chlorpromazine in rats. J. Biochem. Toxicol. 5, 245–251.

Kuntz, E., Liehr, H., Pfingst, W., 1968. Toxic liver damage due to ethionamide. Ger. Med. Mon. 13, 599–602.

Lake, B.G., 1984. Investigations into the mechanism of coumarin-induced hepatotoxicity in the rat. Arch. Toxicol. Suppl. 7, 16–29.

Laurent, G., Kishore, B.K., Tulkens, P.M., 1990. Aminoglycoside-induced renal phospholipidosis and nephrotoxicity. Biochem. Pharmacol. 40, 2383–2392.

Morgan, M.Y., Reshef, R., Shah, R.R., Oates, N.S., Smith, R.L., Sherlock, S., 1984. Impaired oxidation of debrisoquine in patients with perhexiline liver injury. Gut 25, 1057–1064.

Nioi, P., Perry, B.K., Wang, E.J., Gu, Y.Z., Snyder, R.D., 2007. In vitro detection of drug-induced phospholipidosis using gene expression and fluorescent phospholipid based methodologies. Toxicol. Sci. 99, 162–173.

Pelletier, D.J., Gehlhaar, D., Tilloy-Ellul, A., Johnson, T.O., Greene, N., 2007. Evaluation of a published in silico model and construction of a novel bayesian model for predicting phospholipidosis inducing potential. J. Chem. Inf. Model 47, 1196–1205.

Pessayre, D., Bichara, M., Degott, C., Potet, F., Benhamou, J.P., Feldmann, G., 1979. Perhexiline maleate-induced cirrhosis. Gastroenterol. 76, 170–177.

Pessayre, D., Larrey, D., 1988. Acute and chronic drug-induced hepatitis. Baillieres Clin. Gastroenterol. 2, 385–422.

Reasor, M.J., Kacew, S., 2001. Drug-induced phospholipidosis: are there functional consequences? Exp. Biol. Med. 226, 825–830.

Reasor, M.J., Hastings, K.L., Ulrich, R.G., 2006. Drug-induced phospholipidosis: issues and future directions. Expert Opin. Drug Saf. 5, 567–583.

Sawada, H., Takami, K., Asahi, S., 2005. A toxicogenomic approach to drug-induced phospholipidosis: analysis of its induction mechanism and establishment of a novel in vitro screening system. Toxicol. Sci. 83, 282–292.

Sawada, H., Taniguchi, K., Takami, K., 2006. Improved toxicogenomic screening for drug-induced phospholipidosis using a multiplexed quantitative gene expression ArrayPlate assay. Toxicol. In Vitro 20, 1506–1513.

Takashima, K., Mizukawa, Y., Morishita, K., Okuyama, M., Kasahara, T., Toritsuka, N., Miyagishima, T., Nagao, T., Urushidani, T., 2006. Effect of the difference in vehicles on gene expression in the rat liver-analysis of the control data in the Toxicogenomics Project Database. Life Sci. 78, 2787–2796.

Thielemann, L.E., Bosco, C., Rodrigo, R., Orellana, M., Videla, L.A., 1999. Effects of bromoethylamine on antioxidant capacity, lipid peroxidation, and morphological characteristics of rat liver. J. Biochem. Mol. Toxicol. 13, 47–52.

Tomizawa, K., Sugano, K., Yamada, H., Horii, I., 2006. Physicochemical and cell-based approach for early screening of phospholipidosis-inducing potential. J. Toxicol. Sci. 31, 315–324.

Urushidani, T., Nagao, T., 2005. Toxicogenomics: the Japanese initiative. In: Borlak, J. (Ed.), Handbook of Toxicogenomics—Strategies and Applications. Wiley-VCH, pp. 623–631.

Weber, L.W., Boll, M., Stampfl, A., 2003. Hepatotoxicity and mechanism of action of haloalkanes: carbon tetrachloride as a toxicological model. Crit. Rev. Toxicol. 33, 105–136.

Whitehouse, L.W., Menzies, A., Mueller, R., Pontefract, R., 1994. Ketoconazole-induced hepatic phospholipidosis in the mouse and its association with de-*N*-acetyl ketoconazole. Toxicology 94, 81–95.

Xia, Z., Ying, G., Hansson, A.L., Karlsson, H., Xie, Y., Bergstrand, A., DePierre, J.W., Nassberger, L., 2000. Antidepressant-induced lipidosis with special reference to tricyclic compounds. Prog. Neurobiol. 60, 501–512.